



This is a repository copy of *Search for light long-lived neutral particles from Higgs boson decays via vector-boson-fusion production from pp collisions at $\sqrt{s}=13\text{TeV}$ with the ATLAS detector.*

White Rose Research Online URL for this paper:

<https://eprints.whiterose.ac.uk/218479/>

Version: Published Version

Article:

Aad, G. orcid.org/0000-0002-6665-4934, Abbott, B. orcid.org/0000-0002-5888-2734, Abeling, K. orcid.org/0000-0002-1002-1652 et al. (2946 more authors) (2024) Search for light long-lived neutral particles from Higgs boson decays via vector-boson-fusion production from pp collisions at $\sqrt{s}=13\text{TeV}$ with the ATLAS detector. The European Physical Journal C, 84 (7). 719. ISSN 1434-6044

<https://doi.org/10.1140/epjc/s10052-024-12902-7>

Reuse

This article is distributed under the terms of the Creative Commons Attribution (CC BY) licence. This licence allows you to distribute, remix, tweak, and build upon the work, even commercially, as long as you credit the authors for the original work. More information and the full terms of the licence here:

<https://creativecommons.org/licenses/>

Takedown

If you consider content in White Rose Research Online to be in breach of UK law, please notify us by emailing eprints@whiterose.ac.uk including the URL of the record and the reason for the withdrawal request.



eprints@whiterose.ac.uk
<https://eprints.whiterose.ac.uk/>



Search for light long-lived neutral particles from Higgs boson decays via vector-boson-fusion production from pp collisions at $\sqrt{s} = 13$ TeV with the ATLAS detector

ATLAS Collaboration*

CERN, 1211 Geneva 23, Switzerland

Received: 30 November 2023 / Accepted: 9 May 2024 / Published online: 22 July 2024
© CERN for the benefit of the ATLAS Collaboration. 2024

Abstract A search is reported for long-lived dark photons with masses between 0.1 GeV and 15 GeV, from exotic decays of Higgs bosons produced via vector-boson-fusion. Events that contain displaced collimated Standard Model fermions reconstructed in the calorimeter or muon spectrometer are probed. This search uses the full LHC Run 2 (2015–2018) data sample collected in proton–proton collisions at $\sqrt{s} = 13$ TeV, corresponding to an integrated luminosity of 139 fb^{-1} . Dominant backgrounds from Standard Model processes and non-collision sources are estimated using data-driven techniques. The observed event yields in the signal regions are consistent with the expected background. Upper limits on the Higgs boson to dark photon branching fraction are reported as a function of the dark photon mean proper decay length or of the dark photon mass and the coupling between the Standard Model and the potential dark sector. This search is combined with previous ATLAS searches obtained in the gluon–gluon fusion and WH production modes. A branching fraction above 10% is excluded at 95% CL for a 125 GeV Higgs boson decaying into two dark photons for dark photon mean proper decay lengths between 173 and 1296 mm and mass of 10 GeV.

1 Introduction

Many theories beyond the Standard Model (BSM) predict the existence of dark sectors that are weakly coupled to the Standard Model (SM) [1–4]. Depending on how the dark sector is structured and how it couples to the SM, unstable dark states could potentially be generated at colliders, which could then decay into SM particles with significant branching fractions.

The scenario explored in this paper introduces a dark photon (γ_d), acting as the mediator of a broken dark U(1) gauge interaction in the dark sector, and mixing kinetically with

the SM hypercharge. These dark photons can be produced in the exotic decay of the Higgs boson and subsequently decay into pairs of leptons and light quarks [5–7]. The latest LHC measurements on the Higgs boson properties do not rule out decays to yet undetected states with a potentially sizable branching ratio of up to 12% [8]. The mean proper lifetime (τ) of the γ_d is inversely proportional to the mass of the dark photon and to the square of the kinetic mixing parameter (ϵ) [9, 10], which is theoretically allowed to vary over values $\epsilon \lesssim 10^{-2}$. This study focuses on the dark photons with masses in the $\mathcal{O}(\text{MeV}–\text{GeV})$ range and small values of ϵ ($< 10^{-5}$), where decays of the γ_d can occur at a macroscopic distance from their production point.

The decay branching fractions of a light dark photon with kinetic mixing with the SM photon depend on its mass [6, 10, 11]. Dark-photon masses smaller than twice the electron mass result in an invisible Higgs signature and are not considered in this paper. In the range between twice the electron mass and twice the muon mass, the dark photon decays exclusively into electrons, while below twice the pion mass, it decays with equal probability into pairs of muons and electrons. In the range above twice the pion mass, dark photons can decay to electrons, muons, and hadrons, where decay branching fractions vary as a function of the mass due to the presence of hadronic resonances [12]. Due to the large Lorentz boosts expected for dark photons produced with small masses relative to the energy scale of the hard-scattering process, their decay products are expected to be a collimated group of fermions forming a structure similar to a jet, which is referred to as dark-photon jets (DPJs).

The Falkowski–Ruderman–Volansky–Zupan (FRVZ) model [6, 7] is used to optimise event selection and interpret the results. In this model, a pair of dark fermions f_d is produced through a Higgs boson decay and each decays promptly into a dark photon and a stable dark fermion, assumed to be the undetected hidden lightest stable particle (HLSP). This leads to final states with two dark photons

* e-mail: atlas.publications@cern.ch

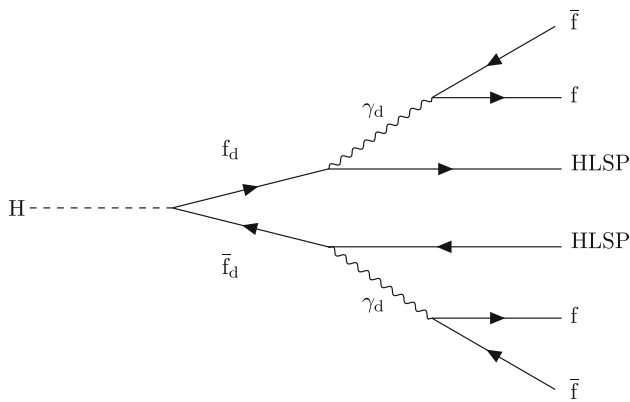


Fig. 1 FRVZ process in Higgs boson decays, with the dark fermion f_d decaying into a γ_d and an HLSP. The γ_d decays into SM fermions, denoted by f and \bar{f}

as shown in Fig. 1. The Higgs boson is assumed to be SM-like with a mass of 125 GeV.

The Hidden Abelian Higgs Model (HAHM) [4], which predicts a direct decay of the Higgs boson into a pair of γ_d , and commonly used as an alternative model to the FRVZ is not considered. This omission is due to the lack of intrinsic missing transverse momentum in such signal events, which limits the analysis sensitivity. Dark-sector radiation [13] can produce additional dark photons in proportion to the size of the dark gauge coupling α_d [5]. To limit the amount of additional γ_d emissions, a dark coupling $\alpha_d \lesssim 0.01$ is assumed in this paper. Despite not making explicit use of this signal feature, the analysis remains sensitive to new physics scenarios that involve multiple γ_d emissions due to the inclusive number of constituents within the DPJ. However, specific interpretation for these scenarios are not provided.

The search for displaced DPJs presented uses the data sample collected at the Large Hadron Collider (LHC) by the ATLAS detector during 2015–2018 in proton–proton (pp) collisions at $\sqrt{s} = 13$ TeV, corresponding to an integrated luminosity of 139 fb^{-1} . Previous ATLAS searches for displaced DPJs were performed using pp collision data at centre-of-mass energies of both 8 TeV [14, 15] and 13 TeV [16, 17], exploring the gluon–gluon fusion (ggF) and WH production modes. These searches provide complementary results to those from related ATLAS searches for prompt DPJs [18–20] probing higher values of ϵ , and for displaced dimuon vertices [21] targeting larger γ_d mass values. Related searches for dark photons were conducted by the CDF and D0 collaborations at the Tevatron [22–24] and by the CMS [25–28], and LHCb [29, 30] collaborations at the LHC. A wide range of constraints on dark photon productions can also be extracted from beam-dump and fixed-target experiments [31–41], e^+e^- collider experiments [42–50], electron and muon anomalous magnetic moment measurements [51–53], and astrophysical observations [54, 55].

Building on the Run 2 ATLAS search for displaced DPJs [17], this paper reports for the first time studies using the vector-boson-fusion (VBF) Higgs-boson production mechanism. This leads to a distinctive topology, characterised by a pair of highly energetic quark-induced jets separated by a significant pseudorapidity gap, resulting in a large invariant mass. Due to the reduction of SM backgrounds in the VBF channel, signal regions requiring as few as one DPJ are feasible, extending the sensitivity to dark photons with shorter and longer decay lengths ($c\tau$). A statistical combination with the ggF and WH production channels [17] is performed to maximise the search sensitivity to the FRVZ model.

2 ATLAS detector

The ATLAS detector [56] at the LHC covers nearly the entire solid angle around the collision point.¹ It consists of an inner tracking detector surrounded by a thin superconducting solenoid, electromagnetic and hadron calorimeters, and a muon spectrometer incorporating three large superconducting air-core toroidal magnets.

The inner-detector system (ID) is immersed in a 2T axial magnetic field and provides charged-particle tracking in the range $|\eta| < 2.5$. The high-granularity silicon pixel detector covers the vertex region and typically provides four measurements per track, the first hit normally being in the insertable B-layer (IBL) installed before Run 2 [57, 58]. It is followed by the silicon microstrip tracker (SCT), which usually provides eight measurements per track. These silicon detectors are complemented by the transition radiation tracker (TRT), which enables radially extended track reconstruction up to $|\eta| = 2.0$. The TRT also provides electron identification information based on the fraction of hits (typically 30 in total) above a higher energy-deposit threshold corresponding to transition radiation.

The calorimeter system covers the pseudorapidity range $|\eta| < 4.9$. Within the region $|\eta| < 3.2$, electromagnetic calorimetry is provided by barrel and endcap high-granularity lead/liquid-argon (LAr) calorimeters, with an additional thin LAr presampler covering $|\eta| < 1.8$ to correct for energy loss in material upstream of the calorimeters. Hadron calorimetry is provided by the steel/scintillator-tile calorimeter, segmented into three barrel structures within $|\eta| < 1.7$, and two copper/LAr hadron endcap calorimeters.

¹ ATLAS uses a right-handed coordinate system with its origin at the nominal interaction point (IP) in the centre of the detector and the z -axis along the beam pipe. The x -axis points from the IP to the centre of the LHC ring, and the y -axis points upwards. Cylindrical coordinates (r , ϕ) are used in the transverse plane, ϕ being the azimuthal angle around the z -axis. The pseudorapidity is defined in terms of the polar angle θ as $\eta = -\ln \tan(\theta/2)$, and the rapidity is defined as $y = (1/2)[(E + p_z)/(E - p_z)]$.

The solid angle coverage is completed with forward copper/LAr and tungsten/LAr calorimeter modules optimised for electromagnetic and hadronic energy measurements respectively.

The muon spectrometer (MS) comprises separate trigger and high-precision tracking chambers measuring the deflection of muons in a magnetic field generated by the superconducting air-core toroidal magnets. The field integral of the toroids ranges between 2.0 and 6.0 Tm across most of the detector. Three layers of precision chambers, each consisting of layers of monitored drift tubes, cover the region $|\eta| < 2.7$, complemented by cathode-strip chambers in the forward region, where the background is highest. The muon trigger system covers the range $|\eta| < 2.4$ with resistive-plate chambers in the barrel, and thin-gap chambers in the endcap regions.

Interesting events are selected by the first-level trigger system implemented in custom hardware, followed by selections made by algorithms implemented in software in the high-level trigger [59]. The first-level trigger accepts events from the 40 MHz bunch crossings at a rate below 100 kHz, which the high-level trigger further reduces in order to record events to disk at about 1 kHz.

An extensive software suite [60] is used in data simulation, in the reconstruction and analysis of real and simulated data, in detector operations, and in the trigger and data acquisition systems of the experiment.

3 Data and simulated event samples

Data were collected using the ATLAS detector during Run 2 of the LHC from 2015 to 2018, at a peak instantaneous luminosity of $2.1 \times 10^{34} \text{cm}^{-2} \text{s}^{-1}$. This resulted in an average of $\langle \mu \rangle = 34$ pp interactions per bunch crossing (pile-up). To ensure the normal operation of all the subdetectors and a stable-collision mode for the LHC beams, data quality requirements were applied. The resulting data sample has an integrated luminosity of $139.0 \pm 2.4 \text{fb}^{-1}$ [61].

In the μ DPJ channel, events were selected using two types of MS-based triggers or unrescaled missing transverse momentum ($E_{\text{T}}^{\text{miss}}$) triggers [62], to target the long-lived γ_{d} decays into muons or signature of the undetected HLSP. The two types of MS-based triggers, ‘tri-muon MS-only’ and ‘muon narrow-scan’ [63] were the same as those developed in the ggF production mode [17]. The narrow-scan trigger efficiencies for signals are independent of the dark photon masses, and found to be 75% and 40% for the 2015–2016 and 2017–2018 data-taking periods, respectively. These values are estimated considering events with γ_{d} decays into muon pairs with $|\eta| < 1.0$ and transverse decay length (L_{xy}) less than 6 m. The tri-muon trigger efficiency varies between 10% and 13%, depending on the dark photon mass.

Unrescaled $E_{\text{T}}^{\text{miss}}$ triggers with the lowest possible threshold were used to search for displaced DPJs decaying into electrons or light hadrons where triggering on the DPJ itself is difficult, and to enhance signal acceptance for the displaced DPJs decaying into muons. Initially, a threshold of 70 GeV was used in 2015, but it was raised multiple times afterwards to account for the increasing effects of multiple pp interactions in the same and neighbouring bunch crossings. By the end of the 2017–2018 data-taking period, the threshold was raised to 110 GeV.

During pp collisions at the LHC, two counter-rotating proton beams are circulated, consisting of bunches of protons. However, not all bunch slots are necessarily filled with protons after LHC injection, with the number of unfilled bunches dependent on the LHC filling scheme [64]. An empty bunch crossing occurs when neither beam contains protons. During empty bunch crossings, a data sample enriched in cosmic-ray muon background is collected (the ‘cosmic data sample’). Additionally, the empty bunches are required to be separated from filled bunches by at least five bunches on each side. A beam-induced background (BIB) [65] enriched data sample (the ‘BIB data sample’) is collected during unpaired isolated bunch crossings. Unpaired bunch crossings happen when only one of the two beams is filled with protons. Additionally, unpaired bunches are required to be separated from filled bunches by at least three unfilled bunches on each side.

Monte Carlo (MC) simulated event samples are used to model the BSM signals. The signal process, where dark photons are produced from the decays of a 125 GeV Higgs boson, is simulated at leading-order (LO) accuracy in α_{S} with MADGRAPH5_AMC@NLO 2.2.3 [66] for the matrix element (ME) calculation, interfaced to PYTHIA 8.186 [67] for parton showering (PS) and hadronisation. The NNPDF2.3LO [68] parton distribution function (PDF) set is utilised. The SM cross-section for the VBF Higgs production of $3.78 \pm 0.08 \text{pb}$ [69] corresponding to $m_{\text{H}} = 125.09 \text{GeV}$, is assumed. Effects of higher-order QCD corrections on the p_{T} of the Higgs boson are evaluated using a reweighting procedure [70]. The impact of these effects on the signal selection efficiency is found to be less than the MC statistical accuracy, and not accounted for in the analysis. The mean proper decay length $c\tau$ of the γ_{d} is considered a free parameter. In the simulated samples, $c\tau$ was chosen to ensure that, accounting for the boost of the γ_{d} , a significant fraction of the decays occur inside the sensitive ATLAS detector volume (up to the second precision layer in the MS at 7 m in radius and 13 m along the z -axis from the centre of the detector). The mass of f_{d} was chosen to be much smaller than the Higgs boson mass and far from the kinematic threshold at $m_{\text{HLSP}} + m_{\gamma_{\text{d}}} = m_{f_{\text{d}}}$. The values of m_{HLSP} and $m_{f_{\text{d}}}$ have a negligible impact on the analysis results provided that m_{HLSP} is much smaller than m_{H} . The mass of the γ_{d} is chosen to be less than twice the values of m_{HLSP} to ensure that it will decay exclusively into SM lep-

tons and light quarks, with the branching fractions depending on its mass. For example, with a mass of 0.4 GeV, the expected dark photon decay branching ratios are 45% e^+e^- , 45% $\mu^+\mu^-$, and 10% $q\bar{q}$ [6].

The largest backgrounds come from multijet, $W +$ jets, $Z +$ jets, $t\bar{t}$, and single-top-quark productions. Data-driven techniques are used to estimate these backgrounds, with MC simulated samples used assisting in validation, uncertainty evaluation, and the training of dedicated multivariate classifiers. The multijet events were simulated using PYTHIA 8.210 [71] with the same set of tuned parameter values (tune) and PDF used for the signal samples. The W +jets and Z +jets samples were simulated using SHERPA 2.2.1 [72] with the NNPDF3.0NNLO [73] PDF set. The single-top and $t\bar{t}$ productions were simulated using POWHEG BOX v2 [74] and PYTHIA 8.230 with the A14 tune [75] for PS and hadronisation, and the NNPDF2.3LO set of PDFs.

Finally, MC samples of $J/\psi \rightarrow \mu\mu$ events were used to estimate systematic uncertainties for muon trigger and reconstruction efficiencies. These samples were simulated using PYTHIA8 + PHOTOS++ [76] with the A14 tune [75] for PS and hadronisation, and the CTEQ6L1 [77, 78] PDF set.

All MC events went through a full simulation of the ATLAS detector geometry and response [79] using the GEANT4 [80] toolkit, taking into account of pile-up and detector response to interactions occurring in neighbouring bunch crossings from the one producing the hard interaction. To model the effects of pile-up, simulated inclusive pp events (PYTHIA 8.210 with the A3 tune [81] and the NNPDF2.3LO set of PDFs), were overlaid on each generated hard-scatter event and reweighted to match the conditions of the 2015–2018 data taking. Reconstructed events are reweighted to reproduce the measured distributions of the number of simultaneous interactions in different data-taking periods. Variations in the trigger threshold as a function of the data taking period are also included in simulation. Corrections were applied to simulated events to ensure agreement with the object, trigger and identification efficiencies determined from control samples in data.

4 Event reconstruction

The analyses presented in this paper use the same reconstruction and identification methods for the physics objects as in the DPJ searches in the ggF and WH production channels [17].

Candidate events are required to have at least one vertex [82] reconstructed from at least two tracks with p_T larger than 500 MeV that are consistent with originating from the beam collision region in the x – y plane. The vertex with the highest sum of squared transverse momenta of associated tracks is considered as the primary vertex of the event.

Jets are reconstructed by combining three-dimensional energy clusters measured by the calorimeter [83] using the anti- k_r jet clustering algorithm [84, 85] with a radius parameter of $R = 0.4$. The standard jet calibration is applied using corrections derived from MC simulation and in situ measurements [86]. In this analysis, jets must have $p_T > 20$ GeV and $|\eta| < 4.9$, and to meet fundamental quality criteria designed to reject detector noise and non-collision backgrounds [87]. Jets containing b -hadrons, also known as b -jets, are identified through a multivariate discriminant that uses track properties [88, 89], with a working point that has 70% efficiency for b -jets from top quark decays. The corresponding rejection factor of light-quark and gluon jets, defined as the inverse of efficiency, is approximately 300; the corresponding factors for jets containing c -hadrons and hadronically decaying τ -leptons are around 38 and 8, respectively.

Electron candidates are reconstructed by combining isolated energy deposits in the electromagnetic calorimeter with ID tracks. To be considered, electrons must satisfy the following criteria: $|\eta| < 2.47$, a transverse momentum $p_T > 20$ GeV, and satisfy the ‘Tight’ requirement, as defined in Ref. [90]. Muon candidates are reconstructed in the range of $|\eta| < 2.5$ by matching tracks in the MS with those in the ID. To be considered as muons, they must meet the following criteria: a transverse momentum $p_T > 20$ GeV and satisfy the ‘Medium’ identification requirements as defined in Ref. [91]. For both the electron and muon candidates, the matched tracks are required to have a significance of the transverse impact parameter, $|d_0|/\sigma(d_0) < 5(3)$, for electrons (muons).² The longitudinal impact parameter z_0 , must satisfy $|z_0 \sin \theta| < 0.5$ mm, where θ corresponds to the polar angle of the track relative to the beam-line. Isolation criteria, based on the scalar sum of p_T of ID tracks, are further applied to both the electrons and muons as in Ref. [17]. To resolve ambiguities that can arise from the independent reconstruction of electron, muon and jet candidates in the detector, the same overlap removal procedures as in Ref. [17] are applied.

The missing transverse momentum vector, \vec{p}_T^{miss} , with magnitude, E_T^{miss} , is calculated as the negative vector sum of the transverse momenta of all identified electrons, muons, and jets, along with an additional component called the ‘soft term’. The soft term is constructed using all tracks originating from the primary vertex that are not matched to any identified lepton or jet. This approach ensures that E_T^{miss} is adjusted to achieve the most accurate calibration of leptons and jets, while simultaneously suppressing contributions from pile-up interactions by excluding them from the soft term [92, 93].

² The transverse impact parameter, d_0 , is defined as the distance of closest approach of a track to the beam-line, measured in the transverse plane with an error $\sigma(d_0)$. The longitudinal impact parameter, z_0 , corresponds to the z -coordinate distance between the point along the track at which the transverse impact parameter is defined and the primary vertex.

4.1 Muonic dark-photon jets

A dark photon decaying into muons outside the ID is expected to generate two or more collimated standalone MS tracks, commonly referred to as a ‘muonic dark-photon jet’ μ DPJ. Standalone MS tracks [91] are reconstructed in the region of MS coverage where the pseudorapidity is $|\eta| \geq 0.1$. These tracks are formed by identifying at least two matched segments in the MS and are then fit with a primary vertex constraint. Although displaced, the muons are expected to point to the PV due to the large boost. Candidates with an absolute value of the pseudorapidity ranging from 1.0 to 1.1 are excluded to avoid the transition region of the MS between the barrel and endcap. Additionally, only standalone MS tracks falling in the pseudorapidity interval $|\eta| < 2.5$, which corresponds to the ID coverage, are selected to allow the computation of an isolation variable based on ID tracks. Standalone MS tracks are required not to match any prompt muon candidate, to discard muons originating from the primary interaction vertex.

The μ DPJs are reconstructed by a Cambridge–Aachen clustering algorithm [94], combining all the selected standalone MS tracks that lie inside a fixed-size cone in the (η, ϕ) space. The reconstruction process begins with the highest- p_T standalone MS track and proceeds by searching for additional standalone MS tracks inside a cone of radius $\Delta R = 0.4$ around the initial track’s momentum vector. If a second standalone MS track is found inside this cone, the axis of the cone is adjusted to the vector sum of the momenta of the two tracks. This process is repeated iteratively until no further tracks are found inside the cone. The μ DPJs are required to contain a minimum of two MS tracks and are discarded if a jet is found within a distance of $\Delta R = 0.4$. This last requirement ensures that μ DPJs remain distinct from other types of dark-photon jets.

Cosmic-ray muons that cross the detector in time coincidence with a pp interaction constitute the main source of background in the μ DPJ. A dense neural network (DNN), referred to as the cosmic-ray tagger, is used to discriminate signal μ DPJs and reject the μ DPJ candidates that originate from the cosmic-ray background. The DNN is implemented using Keras with the Tensorflow backend [95], with its training setup and performance detailed in Ref. [17]. The selection was optimised to obtain a background rejection of 90% while retaining a high signal efficiency. Signal μ DPJs are selected with an efficiency greater than 95% for transverse decay lengths L_{xy} up to 5 m and for γ_d transverse momentum larger than 20 GeV.

4.2 Calorimeter dark-photon jets

A dark-photon decaying into electron or quark pairs in the hadronic calorimeters results in energy deposits that are

reconstructed as a single jet with a low electromagnetic fraction (EMF), defined as the ratio of the energy deposited in the EM calorimeter to the total jet energy. Jets with an EMF below 0.4 are referred to as calorimeter dark-photon-jet candidates caloDPJs. Low EMF jets are reconstructed and calibrated using the same algorithms mentioned earlier for standard jets. However, they are only considered if they have $p_T > 20$ GeV and lie in the range of $|\eta| < 2.5$. Candidates in the transition region between the barrel calorimeters and the endcap cryostat are removed by requiring the fraction of energy in the Tile Gap scintillators to be less than 10% of the total jet energy.

To maintain high efficiency for the targeted signals, low EMF jets are required to satisfy quality criteria that are less stringent than those in the standard jet selection. To reject fake caloDPJs arising from prompt jets, low EMF jets with more than 40% of matched tracks compatible with originating from the primary vertex, as defined by the jet vertex tagger (JVT) [96] are removed. Further caloDPJs cleaning is applied as detailed in Ref. [17] to reject background from noise bursts [97]. These cleaning requirements result in the rejection of approximately 0.8% of low EMF jets in the signal samples.

The time matched to a caloDPJ, denoted by t_{caloDPJ} , is measured as the energy-weighted average of the timing for each calorimeter cell matched to the jet, corrected by the corresponding time-of-flight from the interaction point. It is used to reject cosmic-ray muons and BIB by requiring events from pp collisions to have a value of $|t_{\text{caloDPJ}}|$ that is in a window of 4 ns around zero.

To reduce fake caloDPJs arising from prompt jets, a dedicated discriminator (QCD tagger), based on a convolutional neural network implemented using Keras with the Tensorflow backend, is used to assign a score to each caloDPJ in the event. The training of the neural network and its setup are discussed in Ref. [17]. The QCD tagger inputs are three-dimensional representations of energy deposits matched to the jet. The energy deposits are defined by collections of calorimeter cell clusters used in jet reconstruction [98]. Each collection has (η, ϕ) coordinates and holds information about the total amount of energy deposited in each of the calorimeter samplings. A caloDPJ is accepted if the QCD tagger output is larger than 0.5, indicating an enhanced probability of a displaced signature. This corresponds to a selection efficiency of more than 70% for γ_d with transverse decay lengths L_{xy} in the range of 2–3.5 m and p_T larger than 20 GeV, with a background rejection of 94% [17].

Muons arising from BIB can deposit energy in the HCAL by radiative losses, which can be reconstructed as caloDPJs owing to the resulting low EMF. To reduce the residual contamination from misidentified caloDPJs from BIB, a dedicated per-jet tagger (BIB tagger) as detailed in Ref. [17] is used. The selection is optimised to obtain a signal efficiency

of greater than 80% with a corresponding BIB rejection of 68%.

5 Event selection and background estimate

Long-lived dark photon candidate events are selected by requiring at least one DPJ satisfying the selection criteria described in Sect. 4. If more than one DPJ is reconstructed, only the one with the highest transverse momentum, called the ‘leading DPJ’, is considered and used to classify the event into two exclusive categories, caloDPJs and μ DPJs, based on its type. In the μ DPJ channel, events are triggered by the logical OR of the dedicated muon triggers (tri-muon and narrow-scan) and the E_T^{miss} trigger as discussed in Sect. 3, to target both the displaced muonic signature and the large E_T^{miss} in the FRVZ signal models. In the caloDPJ channel, events are triggered by the E_T^{miss} trigger.

To reject background from SM processes and to select events consistent with the VBF production, events are required to have:

- at least two jets with $p_T \geq 30$ GeV;
- the invariant mass of the two leading jets, $m_{jj} \geq 1000$ GeV;
- the pseudo-rapidity gap between the two leading jets, $|\Delta\eta_{jj}| > 3$;
- the azimuthal angular difference between the two leading jets, $|\Delta\phi_{jj}| < 2.5$;
- exactly zero leptons;
- exactly zero b-tagged jets;
- $E_T^{\text{miss}} \geq 100$ GeV.

The centrality in pseudo-rapidity of the DPJ between the two VBF jets, C_{DPJ} , is used to enhance the analysis sensitivity in the μ DPJ channel. It is defined as:

$$C_{\text{DPJ}} = \exp\left(-\frac{4}{(\eta_{j1} - \eta_{j2})^2} \left(\eta_{\text{DPJ}} - \frac{\eta_{j1} + \eta_{j2}}{2}\right)^2\right).$$

In the μ DPJ signal region (SR), SR_μ , the value of C_{DPJ} is required to be greater than 0.7, to capture the VBF topology where the DPJ is centred between the two VBF jets. To further reduce the multijet background events in the caloDPJ channel, the minimum azimuthal distance between the \vec{p}_T^{miss} and the \vec{p}_T of each of the four leading jets in the event, $\Delta\phi_{\text{min}}$, is required to be greater than 0.4 to reject events with mis-measured jet energies leading to fake E_T^{miss} in the event.

To improve the analysis sensitivity, the caloDPJ final state is further split into two exclusive SRs, SR_c^L and SR_c^H , where E_T^{miss} is in the range of [100, 225] GeV and E_T^{miss} is > 225 GeV, respectively. Table 1 summarises the selections applied in all three SRs. Further selections, as shown in

Table 1 Definition of the signal regions in the μ DPJ and caloDPJ channels. Selections on the DPJ are applied only to the leading one. The caloDPJ final state is further split into two signal regions, SR_c^L , and SR_c^H , with E_T^{miss} values of $\in [100, 225]$ GeV and > 225 GeV respectively. Dashes indicate cases where a requirement is not applied

Requirement/region	SR_μ	$\text{SR}_c^{L/H}$
Number of DPJs	≥ 1	≥ 1
Leading DPJ type	μ DPJ	caloDPJ
Trigger	E_T^{miss} Tri-muon MS-only Muon narrow-scan	E_T^{miss}
$p_T(\text{jet})$ [GeV]	> 30	> 30
N_{jet}	≥ 2	≥ 2
m_{jj} [GeV]	≥ 1000	≥ 1000
$ \Delta\eta_{jj} $	> 3	> 3
$ \Delta\phi_{jj} $	< 2.5	< 2.5
N_ℓ	0	0
$N_{b\text{-jet}}$	0	0
C_{DPJ}	> 0.7	–
$\Delta\phi_{\text{min}}$	–	> 0.4
E_T^{miss} [GeV]	> 100	SR_c^L : [100, 225] SR_c^H : > 225
$ \mu$ DPJ charge	0	–
caloDPJ QCD tagger	–	> 0.9
$\sum_{\Delta R=0.5} p_T$ [GeV]	< 2	< 2

Table 1, are applied to the leading DPJ to improve the search sensitivity based on the following variables:

- The μ DPJ charge is the sum of the charges of muon-tracks matched to a μ DPJ is sensitive to the charge of the initiating state. μ DPJs originating from neutral particle decays are expected to have zero sum of charge;
- The $\sum_{\Delta R=0.5} p_T$ is the scalar sum of the transverse momenta of all tracks within a $\Delta R = 0.5$ cone around the direction of the DPJ momentum vector. Displaced DPJs are expected to have very little nearby track activity in the ID.

The main sources of background left after the SR selections are punch-through jets from rare multijet events for SR_μ , and multijet and electroweak W and Z production for SR_c^L and SR_c^H .

Non-collision backgrounds, including cosmic-ray muon and BIB, are found to be negligible. The cosmic-ray muon background contribution is estimated from events collected with the analysis triggers in the cosmic data sample. By requiring at least one reconstructed μ DPJ, the contribution from cosmic-ray muon is found to be subdominant. After all selection, it is found to be negligible in all signal regions.

Table 2 Definition of the control regions used in the background estimation. All CRs requirements are the same as for the respective SR, with the exception of the selections reported in this table. End points within the ranges are included (excluded) when denoted by square (round) brackets

Requirement/region	CRB $_{\mu}$	CRC $_{\mu}$	CRD $_{\mu}$
$ \mu\text{DPJ charge} $	[1, 5)	[1, 5)	0
$\sum_{\Delta R=0.5} p_T [\text{GeV}]$	[0, 2.0)	[2.0, 20)	[2.0, 20)
Requirement/region	CRB $_{c}^{L/H}$	CRC $_{c}^{L/H}$	CRD $_{c}^{L/H}$
caloDPJ QCD tagger score	[0.9, 1]	[0.8, 0.9)	[0.8, 0.9)
$\sum_{\Delta R=0.5} p_T [\text{GeV}]$	[2.0, 20)	[2.0, 20)	[0, 2.0)

Events with BIB energy deposits are very likely to have a caloDPJ which can contribute to the background. The possible contribution from misidentified caloDPJs was studied using the BIB-enriched data sample. The BIB contamination is found to be negligible after the timing and BIB tagger requirements. Hence this background contribution in the SR is neglected.

As nearly all background in the SR arises from a prompt jet misidentified as a displaced jet, a common data-driven ‘ABCD’ method is used to estimate their contributions. This method relies on the assumption that the distribution of background events can be factorised in two dimensions using two uncorrelated variables. The background events are then subdivided into four regions: A, B, C, and D. In the ABCD convention, region A is the SR, regions B, C, D are also referred to as control regions CRB, CRC, and CRD. Without any signal contamination in regions B, C, and D, the number of background events in the SR can be estimated as $N_A = N_D \times N_B/N_C$, where $N_{B,C,D}$ are the number of observed events in data in the B, C, and D regions. Any possible signal leakage outside the SR region is accounted for by using a modified ABCD method that simultaneously fits the signal and background events in all regions. The two dimensional distributions used in the estimate of the backgrounds are formed by $\{\mu\text{DPJ charge}, \sum_{\Delta R=0.5} p_T\}$ in the μDPJ channel, and $\{\text{QCD tagger discriminant}, \sum_{\Delta R=0.5} p_T\}$ in the caloDPJ channel. Definitions of the control regions CRB, CRC, and CRD are shown in Table 2. All CRs requirements are the same as for the respective SR, with the exception of the selections reported in this table.

The background estimate procedure was validated by applying the ABCD method in validation regions (VRs), where signal contributions are small. A first set of VRs are obtained by combining control regions as defined in Table 2, such as a combination of CRB and CRC, or a combination of CRC and CRD. To improve the statistical uncertainty, the selection requirements on E_T^{miss} in the μDPJ VRs is relaxed to be greater than 20 GeV, and the VRs in the caloDPJ channel are defined within a common E_T^{miss} range

of $E_T^{\text{miss}} > 100$ GeV. A second set of the VRs are defined by inverting the selections on $\Delta\phi_{jj}$ or $\Delta\phi_{\text{min}}$ in the μDPJ or caloDPJ channel, respectively. To improve the statistical uncertainty in these VRs, the C_{DPJ} selection requirement is removed in the μDPJ channel, and the caloDPJ VRs are defined within a common E_T^{miss} range of $E_T^{\text{miss}} > 100$ GeV.

For each VR, alternative (ABCD)’ test regions are defined, and region boundaries are varied in discrete steps to assess the dependence on the variables used in the ABCD planes. The Pearson linear correlation coefficient between the two variables defining the ABCD plane in all VRs was found to be less than 3% and the signal leakage was found to be less than 1% of the total signal in the SR selection for all signal scenarios considered in the analysis. In the μDPJ VRs, $\sum_{\Delta R=0.5} p_T$ boundaries are tested in the range of 0.5–4.5 GeV or 2.5–7.0 GeV. In the caloDPJ VRs, $\sum_{\Delta R=0.5} p_T$ boundaries are tested in the range of 0.5–4.5 GeV or 2.5–5.5 GeV, and boundaries on the QCD tagger discriminant boundaries are tested in the range of 0.84–0.98 or 0.82–0.88. In all the VRs, the observed yields were found to agree with the estimated background predictions within about one standard deviation considering only the statistical uncertainties in the VRs. The relative statistical uncertainties of the predicted backgrounds in the VRs are about 25% and 15% in the μDPJ and caloDPJ channels, respectively, when using the same boundary definitions as in the SRs.

Figure 2 shows the distribution of data events in the ABCD plane for the μDPJ channel, together with the expected distribution for a benchmark FRVZ model assuming a 125 GeV Higgs boson and a decay branching fraction to the dark sector of 10%. The acceptance times efficiency for the FRVZ signal processes after applying all SR selection criteria is 0.31% in the case of a γ_d mass of 400 MeV and a generated $c\tau$ of 50 mm.

Figure 3 shows the distribution of data events in the ABCD plane for the caloDPJ channels, together with the expected distribution for a benchmark FRVZ model assuming a 125 GeV Higgs boson and a decay branching fraction to the dark sector of 10%. The acceptance times efficiency for the FRVZ signal processes after applying SR selection criteria is 0.093% or 0.032% for SR_{c}^L or SR_{c}^H , in the case of a γ_d mass of 100 MeV and a generated $c\tau$ of 15 mm.

6 Systematic uncertainties

Potential sources of experimental uncertainties are considered for the simulated signal yields to account for potential data and MC differences in the event reconstruction and selections. For the background estimations, the statistical uncertainties in the observed yields in regions CRB, CRC, and CRD are directly propagated to the SR from the ABCD method.

Fig. 2 The per-event μ DPJ charge vs $\sum_{\Delta R=0.5} p_T$ distributions in the ABCD planes defined for the SR_μ . Figure **a** shows events in data, while figure **b** shows simulated FRVZ events, assuming a 125 GeV Higgs boson with a decay branching fraction of 10% to the dark sector and γ_d with mass of 400 MeV and $c\tau = 50$ mm

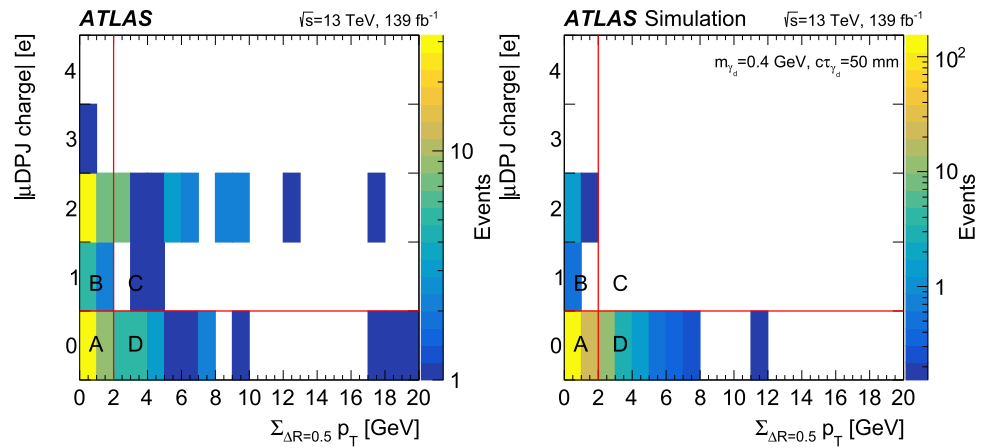
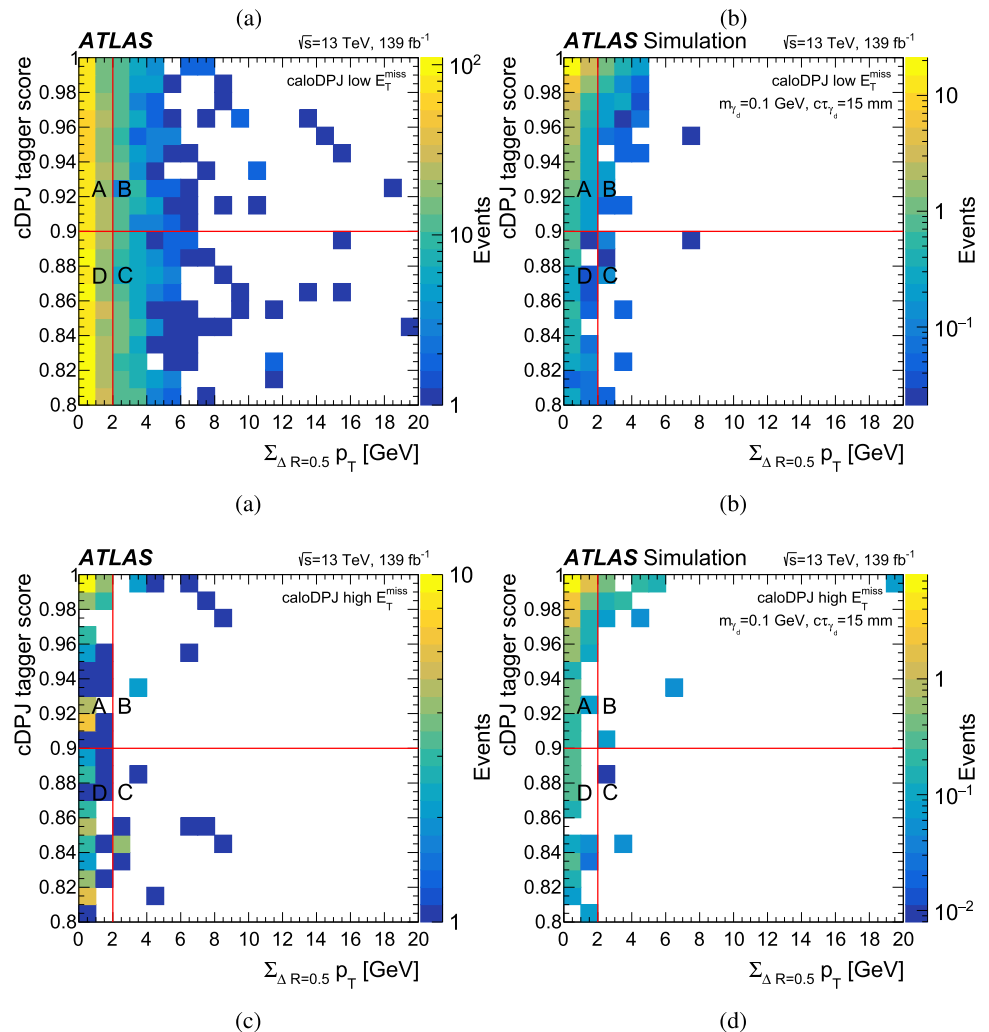


Fig. 3 The per-event QCD tagger vs $\sum_{\Delta R=0.5} p_T$ distributions in the ABCD planes defined for the **a, b** SR_C^L and **b, c** SR_C^H channels. Figures **a, c** show events in data, while figures **b, d** show simulated FRVZ events, assuming a 125 GeV Higgs boson with a decay branching fraction of 10% to the dark sector and γ_d with mass of 100 MeV and $c\tau = 15$ mm



Experimental uncertainties for jets include jet energy scale (JES) and jet energy resolution (JER) uncertainties from the standard calibration scheme [86], which amount to less than 7% of the expected signal yields. An additional JES uncertainty is applied to consider a possible dependence on the low-EM-fraction selection. It is estimated following the

same procedure as used in the 2015–2016 dark-photon jet search [16] and is up to 13% for the caloDPJ channels.

In the μ DPJ channel, a systematic uncertainty in the single- γ_d reconstruction efficiency is evaluated using a tag-and-probe method applied to $J/\psi \rightarrow \mu\mu$ events in data and simulation, taking into account the leading effect from the opening angle ΔR between the two muons. The J/ψ

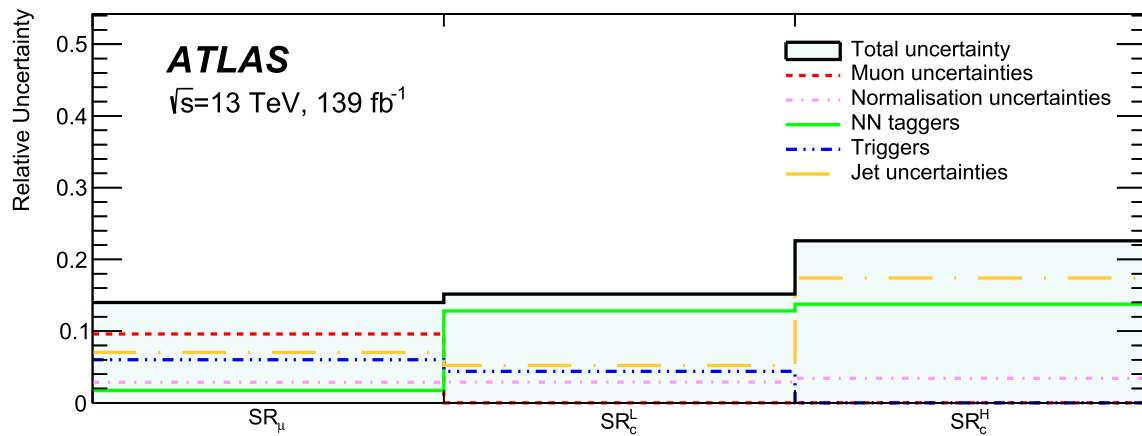


Fig. 4 Comparison of the relative uncertainty in the signal yield in each SR, showing the contributions from the different sources of uncertainty summed in quadrature. The quoted values are averaged over different γ_d masses. The ‘Muon uncertainties’ category contains all muon-related systematic uncertainties and is dominated by the uncertainty in the single- γ_d reconstruction efficiency. The ‘NN taggers’ category contains the three taggers adopted in the analysis and is dominated by the BIB

tagger uncertainties for the calorimetric channels and by the cosmic-ray tagger in the muonic channel. The ‘Triggers’ category contains all trigger systematic uncertainties. The ‘Jet uncertainties’ category contains the JES, JER and low-EM-fraction JES systematic uncertainties. Some sets of systematic uncertainties apply to only a subset of the SRs. The systematic uncertainty in the lifetime extrapolation is not shown

reconstruction efficiency is evaluated in both the data and simulation as a function of the opening angle ΔR between the two muons, and the corresponding difference between data and simulation in the $\Delta R < 0.06$ region, where the DPJ samples are concentrated, is found to be up to 9.6% and taken as the uncertainty.

The systematic uncertainty in the E_T^{miss} trigger efficiency is evaluated by propagating the statistical error of the trigger scale-factors introduced in Sect. 3. It is estimated to be less than 9% and 4% in SR_c^L and SR_μ respectively.

The uncertainties related to the MC modelling of the taggers are obtained from Ref. [17] and recalculated for all signal samples. In the case of the cosmic-ray tagger, the calculated uncertainty is found to be less than 4% in SR_μ . Conversely, for the QCD tagger and the BIB tagger, the estimated uncertainties are found to be less than 6% and 12%, respectively, in both the SR_c^L and SR_c^H .

A pile-up modelling uncertainty is assigned to account for the difference between the predicted and measured inelastic cross-sections [99], which is evaluated to be less than 5% in all signal regions.

A systematic uncertainty in the procedure used for extrapolating the signal efficiency to different lifetimes was evaluated by comparing the extrapolated efficiency derived from the main simulated samples with the measured efficiency of samples with alternative lifetime assumptions. The results showed agreement within statistical uncertainties, except for the SR_c^L selection, where the extrapolated efficiency at large lifetime values is lower by 36% from the nominal value. Consequently, a one-sided systematic uncertainty of 36% is

Table 3 Observed and expected yields in the ABCD regions. The total uncertainty in the background expectation is computed by the ABCD background-only fit to unblinded data

Selection	CRB	CRC	CRD	SR expected	SR observed
SR_μ	44	22	21	42 ± 14	41
SR_c^L	224	256	1123	983 ± 95	923
SR_c^H	9	11	35	29 ± 14	46

included when extrapolating events from the SR_c^L region to lifetimes larger than the generated MC lifetime.

Finally, an uncertainty in the computed total integrated luminosity used to rescale the expected number of signal events is considered. The uncertainty in the combined 2015–2018 integrated luminosity is 1.7% [100], obtained using the LUCID-2 detector [101] for the primary luminosity measurements.

Figure 4 summarises the average experimental uncertainties for the bulk of the signal samples, where absolute deviations are found to be on the order of a few percent up to 6% for the total uncertainty across different γ_d masses.

7 Results and interpretations

A combined maximum-likelihood fit to the yields in the four (i.e. ABCD) regions in data is used for data-driven background estimations in each SR and for model interpretations. The likelihood function is constructed as a product of Poisson functions, one for each of the SR, CRB, CRC,

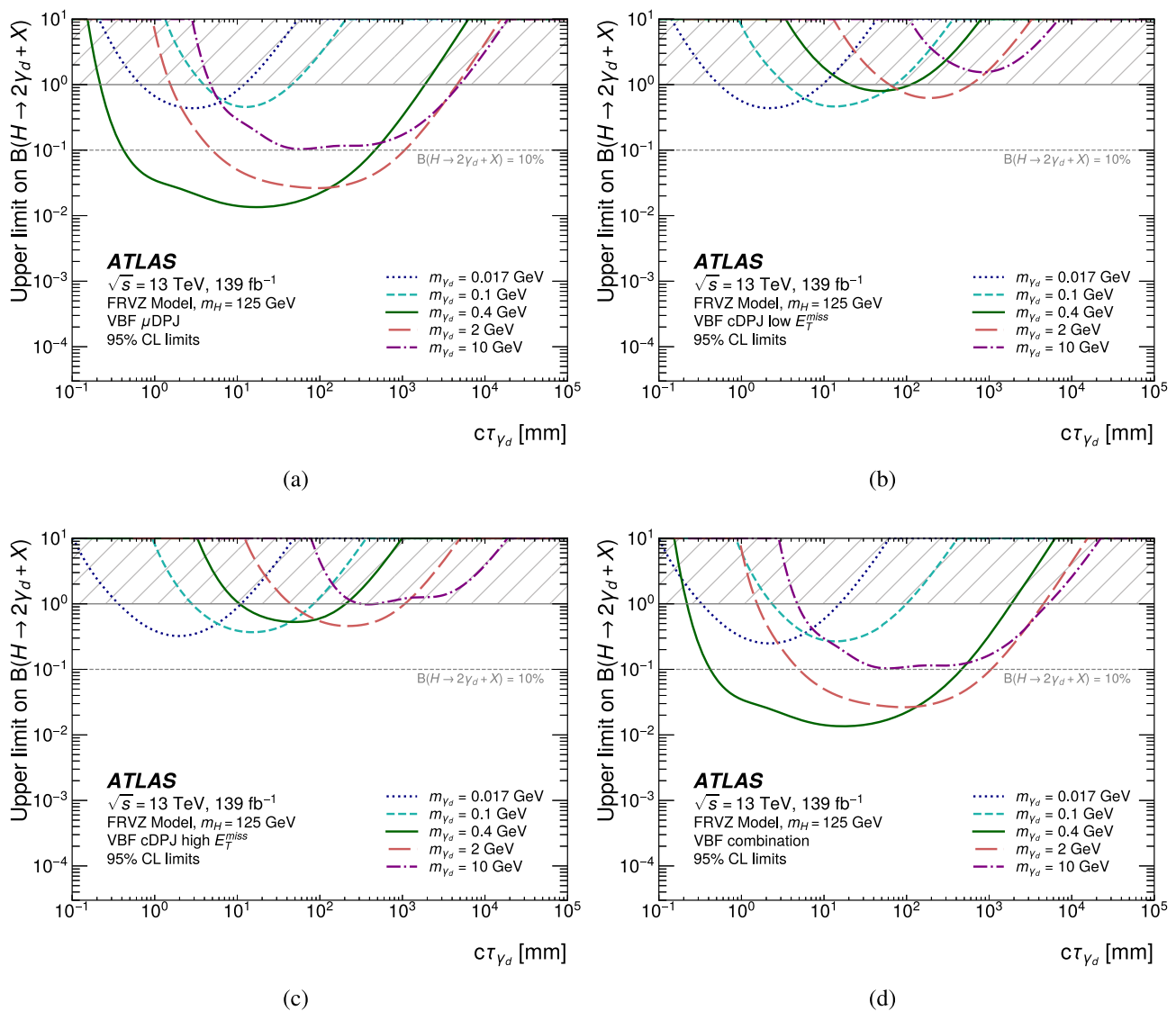


Fig. 5 Upper limits at 95% CL on the branching fraction as a function of the dark-photon mean proper decay length $c\tau$ for the $H \rightarrow 2\gamma_d + X$ process, assuming a 125 GeV Higgs boson and a FRVZ signal model.

and CRD regions, describing signal and background expectations. The ABCD ansatz is introduced as nuisance parameters in the background component of the expected yield in each region. The likelihood-based ABCD fit is robust against control regions with only a few events and considers possible signal contamination in the control regions. Higgs-boson contribution via the ggF mechanism or in association with a vector boson (WH or ZH) are at the percent level, and thus neglected. The effects of systematic uncertainties described in Sect. 6 are treated in the fit by nuisance parameters with Gaussian constraints. These parameters are assumed to be uncorrelated across regions, where an alternative correlation model with full correlation across regions is studied

The limits are shown separately for the **a** SR_μ , **b** SR_μ^L , **c** SR_μ^H search channels, and **d** with all channels combined. The hatched band denotes the region in which the branching ratio is larger than unity

and found to have a negligible impact on the results. The mean value of the Gaussian probability distribution function is constrained by the nominal value of the parameter and the variance is defined by the 68% confidence interval of the systematic uncertainty associated with the parameter.

Table 3 presents the observed and expected numbers of events in all SRs. The reported yields are extrapolated by the fit assuming no signal, and with unblinded data in all ABCD regions in the fit. When comparing the results with a likelihood fit using blinded data in the SR, the background yields are found to be consistent within percent level. No significant excess above expected background is observed.

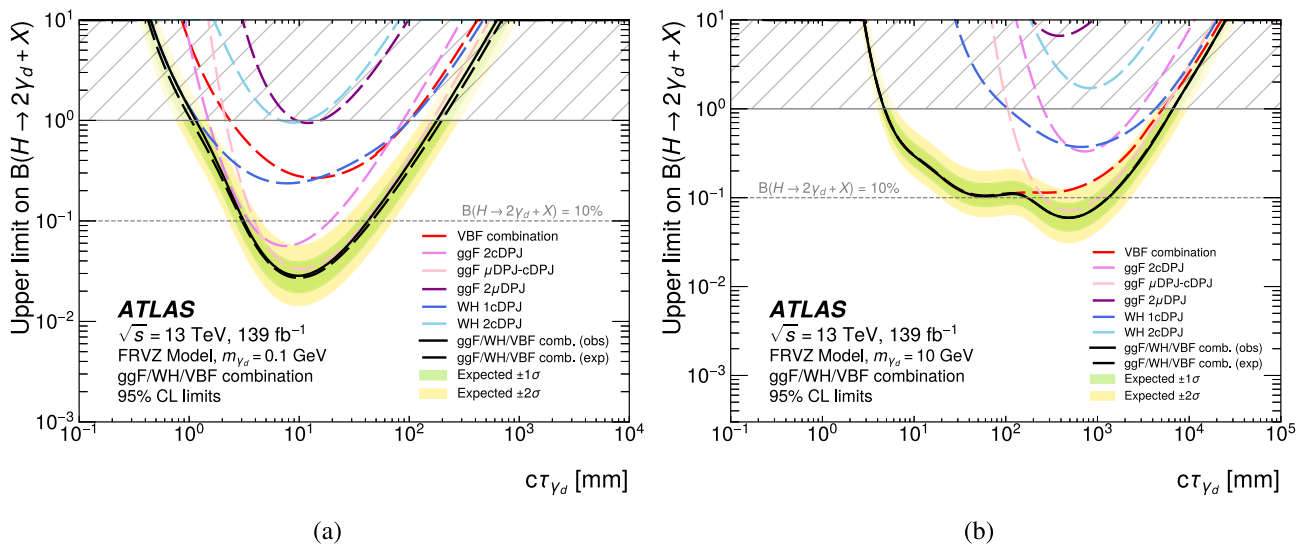
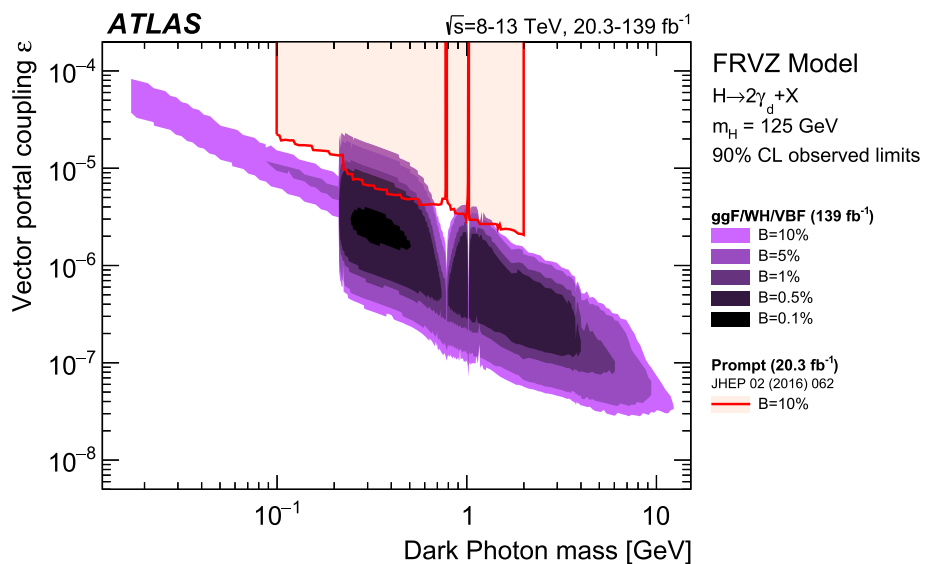


Fig. 6 Upper limits at 95% CL on the branching fraction as a function of the dark-photon mean proper decay length $c\tau$ for the $H \rightarrow 2\gamma_d + X$ process, assuming a 125 GeV Higgs boson and a FRVZ signal model. The limits are shown separately for each channel and for the statistical

combination (solid black) for a γ_d mass of **a** 100 MeV and **b** 10 GeV. The hatched band denotes the region in which the branching ratio is larger than unity

Fig. 7 90% CL exclusion contours of the $B(H \rightarrow 2\gamma_d + X)$ as a function of the γ_d mass and the kinetic mixing parameter ϵ . These limits are obtained assuming branching fractions between 0.1% and 10% (shown as distinct shades of purple within the contour regions) for Higgs boson decays resulting in dark photons. The figure also shows the region excluded by the previous ATLAS search for prompt [20] (solid red line) decays of dark photons



The results are then used to set upper limits on the branching fraction $B(H \rightarrow 2\gamma_d + X)$ as a function of the γ_d mean proper decay length $c\tau$, assuming the SM VBF production cross section of a 125 GeV Higgs boson, with X assumed to be undetected. The upper limit on the signal strength, relative to the predicted signal yields from simulation, is obtained with the CL_s method [102] with the asymptotic calculator [103]. The validity of the asymptotic approximation is checked against a full calculation using pseudo-experiments, and the CL_s values of the two methods typically agree within 5%.

Figure 5 shows a summary of the observed limits on the branching ratio $B(H \rightarrow 2\gamma_d + X)$ assuming the production

of a 125 GeV Higgs boson. The sensitivity of each SR and the combination are reported in separate subfigures for the VBF production. In the region where γ_d masses are less than twice the muon mass, dark photons can decay into electrons and light quarks within the muon spectrometer volume and are reconstructed as μ DPJ. Sensitivities in the μ DPJ channel are typically much better than the caloDPJ channels due to the larger signal efficiency, except in the region where dark photon masses are below twice the muon mass. The high E_T^{miss} region in the caloDPJ channel mainly contributes in scenarios involving dark photons with masses larger than 10 GeV and large $c\tau$ values, where one of the dark photons may decay outside ATLAS.

The results in the VBF analysis are then combined with the SRs in the ggF and WH analyses [17], constructed to be mutually exclusive by different selections on the m_{jj} and the number of prompt leptons. The combined fit considers a product of the likelihood functions of the individual search channels with independent nuisance parameters, but with a common signal normalisation. Systematic uncertainties in the SRs are assumed to be fully uncorrelated. In each production channel, contributions from other Higgs boson productions are relatively small, and not considered as signal for simplicity. Figure 6 shows the expected and observed limits on $B(H \rightarrow 2\gamma_d + X)$ for a γ_d mass of 0.1 and 10 GeV, as functions of the dark photon mean proper decay length $c\tau$, combining all production channels. Observed limits in different SRs used in the combination are also presented for comparison. The VBF channel contributes significantly to the sensitivity for the dark photons with short and long decay lengths. Branching fractions larger than 5% can be excluded at 95% CL if the dark photons have a mean proper decay length $c\tau$ between 1 mm and 5 mm and a mass below twice the muon mass. For the scenarios where dark photon masses are between 0.4 GeV and 6 GeV, branching fractions larger than 1% can be excluded at 95% CL if the dark photons have a mean proper decay length $c\tau$ between 1 mm and 267 mm. For the dark photons with masses of 10 GeV, branching fractions larger than 10% are excluded at 95% CL if the dark photons have a mean proper decay length $c\tau$ between 173 mm and 1296 mm.

Upper limits at 90% CL³ are also set, in the context of the FRVZ model in terms of kinetic mixing parameter ϵ and γ_d mass and presented in Fig. 7 for different $B(H \rightarrow 2\gamma_d + X)$, ranging from 0.1% to 10%. The limits are interpolated between different masses by branching fraction variations [10] as a function of the γ_d mass, corrected by a linear interpolation of the signal efficiency between adjacent available MC signal samples. For a γ_d mass below twice the muon mass, no coverage from μ DPJ signal regions is expected, motivating a significant drop in sensitivity.

8 Conclusion

A search for long-lived dark photons decaying into collimated pairs of fermions is performed using 139 fb^{-1} of data collected from pp collisions at $\sqrt{s} = 13 \text{ TeV}$ at the ATLAS detector. The analysis considers the FRVZ signal models where dark photons are produced from Higgs boson decays. The VBF topology, which is characterised by two energetic jets that have a large rapidity separation in addition to large

values of m_{jj} and E_T^{miss} is studied for the first time to target the VBF Higgs boson production mode. The reduction of background in the VBF channel makes it feasible to require only one long-lived dark photon candidate in the events, sensitive to the dark photons with shorter or longer decay lengths where one of the dark photons may decay promptly or outside ATLAS and escape the DPJ reconstruction. The data are found to be consistent with the background prediction. Upper limits on $B(H \rightarrow 2\gamma_d + X)$ as a function of dark photon mass and mean proper decay length $c\tau$ are reported, assuming the SM cross-section for a 125 GeV Higgs boson.

This search is also combined with previous ATLAS searches obtained in the gluon–gluon fusion and WH production modes [17]. Branching fractions above 10% can be excluded at 95% CL for $H \rightarrow 2\gamma_d + X$ decays for dark photons with mean proper decay length between 173 and 1296 mm and mass of 10 GeV, compared with the range of [263–1030] mm in the previous publication [17]. The improvement is entirely due to the addition of the VBF channel and the statistical combination.

Acknowledgements We thank CERN for the very successful operation of the LHC and its injectors, as well as the support staff at CERN and at our institutions worldwide without whom ATLAS could not be operated efficiently. The crucial computing support from all WLCG partners is acknowledged gratefully, in particular from CERN, the ATLAS Tier-1 facilities at TRIUMF/SFU (Canada), NDGF (Denmark, Norway, Sweden), CC-IN2P3 (France), KIT/GridKA (Germany), INFN-CNAF (Italy), NL-T1 (Netherlands), PIC (Spain), RAL (UK) and BNL (USA), the Tier-2 facilities worldwide and large non-WLCG resource providers. Major contributors of computing resources are listed in Ref. [104]. We gratefully acknowledge the support of ANPCyT, Argentina; YerPhi, Armenia; ARC, Australia; BMWFW and FWF, Austria; ANAS, Azerbaijan; CNPq and FAPESP, Brazil; NSERC, NRC and CFI, Canada; CERN; ANID, Chile; CAS, MOST and NSFC, China; Minciencias, Colombia; MEYS CR, Czech Republic; DNRF and DNSRC, Denmark; IN2P3-CNRS and CEA-DRF/IRFU, France; SRNSFG, Georgia; BMBF, HGF and MPG, Germany; GSRI, Greece; RGC and Hong Kong SAR, China; ISF and Benozio Center, Israel; INFN, Italy; MEXT and JSPS, Japan; CNRST, Morocco; NWO, Netherlands; RCN, Norway; MEiN, Poland; FCT, Portugal; MNE/IFA, Romania; MESTD, Serbia; MSSR, Slovakia; ARRS and MIZŠ, Slovenia; DSI/NRF, South Africa; MICINN, Spain; SRC and Wallenberg Foundation, Sweden; SERI, SNSF and Cantons of Bern and Geneva, Switzerland; MOST, Taipei; TENMAK, Türkiye; STFC, UK; DOE and NSF, United States of America. Individual groups and members have received support from BCKDF, CANARIE, CRC and DRAC, Canada; CERN-CZ, PRIMUS 21/SCI/017 and UNCE SCI/013, Czech Republic; COST, ERC, ERDF, Horizon 2020, ICSC-NextGenerationEU and Marie Skłodowska-Curie Actions, European Union; Investissements d’Avenir Labex, Investissements d’Avenir Idex and ANR, France; DFG and AvH Foundation, Germany; Herakleitos, Thales and Aristeia programmes co-financed by EU-ESF and the Greek NSRF, Greece; BSF-NSF and MINERVA, Israel; Norwegian Financial Mechanism 2014–2021, Norway; NCN and NAWA, Poland; La Caixa Banking Foundation, CERCA Programme Generalitat de Catalunya and PROMETEO and GenT Programmes Generalitat Valenciana, Spain; Göran Gustafssons Stiftelse, Sweden; The Royal Society and Leverhulme Trust, UK. In addition, individual members wish to acknowledge support from Chile: Agencia Nacional de Investigación y Desarrollo (FONDECYT 1190886, FONDECYT 1210400,

³ The limits are quoted at 90% CL in this interpretation of the results to ease the comparison with other experiments that conventionally use this CL threshold.

FONDECYT 1230987); China: National Natural Science Foundation of China (NSFC-12175119, NSFC 12275265); European Union: European Research Council (ERC-948254), Horizon 2020 Framework Programme (MUCCA-CHIST-ERA-19-XAI-00), Italian Center for High Performance Computing, Big Data and Quantum Computing (ICSC, NextGenerationEU), Marie Skłodowska-Curie Actions (EU H2020 MSC IF GRANT NO 101033496); France: Agence Nationale de la Recherche (ANR-20-CE31-0013, ANR-21-CE31-0013, ANR-21-CE31-0022), Investissements d'Avenir Idex (ANR-11-LABX-0012), Investissements d'Avenir Labex (ANR-11-LABX-0012); Germany: Baden-Württemberg Stiftung (BW Stiftung-Postdoc Eliteprogramme), Deutsche Forschungsgemeinschaft (DFG-CR 312/5-1); Italy: Istituto Nazionale di Fisica Nucleare (FELLINI G.A. n. 754496, ICSC, NextGenerationEU); Japan: Japan Society for the Promotion of Science (JSPS KAKENHI 22H01227, JSPS KAKENHI JP21H05085, JSPS KAKENHI JP22H04944); Netherlands: Netherlands Organisation for Scientific Research (NWO Veni 2020-VI.Veni.202.179); Norway: Research Council of Norway (RCN-314472); Poland: Polish National Agency for Academic Exchange (PPN/PPO/2020/1/00002/U/00001), Polish National Science Centre (NCN 2021/42/E/ST2/00350, NCN OPUS nr 2022/47/B/ST2/03059, NCN UMO-2019/34/E/ST2/00393, UMO-2020/37/B/ST2/01043, UMO-2021/40/C/ST2/00187); Slovenia: Slovenian Research Agency (ARIS grant J1-3010); Spain: BBVA Foundation (LEO22-1-603), Generalitat Valenciana (Artemisa, FEDER, IDIFEDER/2018/048), La Caixa Banking Foundation (LCF/BQ/PI20/11760025), Ministry of Science and Innovation (RYC2019-028510-I, RYC2020-030254-I), PROMETEO and GenT Programmes Generalitat Valenciana (CIDEAGENT/2019/023, CIDEAGENT/2019/027); Sweden: Swedish Research Council (VR 2018-00482, VR 2022-03845, VR 2022-04683), Knut and Alice Wallenberg Foundation (KAW 2017.0100, KAW 2018.0157, KAW 2018.0458, KAW 2019.0447); Switzerland: Swiss National Science Foundation (SNSF-PCEFP2_194-658); UK: Leverhulme Trust (Leverhulme Trust RPG-2020-004); USA: Neubauer Family Foundation.

Data Availability Statement This manuscript has no associated data. [Authors' comment: "All ATLAS scientific output is published in journals, and preliminary results are made available in Conference Notes. All are openly available, without restriction on use by external parties beyond copyright law and the standard conditions agreed by CERN. Data associated with journal publications are also made available: tables and data from plots (e.g. cross section values, likelihood profiles, selection efficiencies, cross section limits, ...) are stored in appropriate repositories such as HEPDATA (<http://hepdata.cedar.ac.uk/>). ATLAS also strives to make additional material related to the paper available that allows a reinterpretation of the data in the context of new theoretical models. For example, an extended encapsulation of the analysis is often provided for measurements in the framework of RIVET (<http://rivet.hepforge.org/>)."] This information is taken from the ATLAS Data Access Policy, which is a public document that can be downloaded from <http://opendata.cern.ch/record/413> [opendata.cern.ch].]

Code Availability Statement This manuscript has no associated code/software. [Authors' comment: "All ATLAS scientific output is published in journals, and preliminary results are made available in Conference Notes. All are openly available, without restriction on use by external parties beyond copyright law and the standard conditions agreed by CERN. Data associated with journal publications are also made available: tables and data from plots (e.g. cross section values, likelihood profiles, selection efficiencies, cross section limits, ...) are stored in appropriate repositories such as HEPDATA (<http://hepdata.cedar.ac.uk/>). ATLAS also strives to make additional material related to the paper available that allows a reinterpretation of the data in the context of new theoretical models. For example, an extended encapsulation of the analysis is often provided for measurements in the framework of RIVET (<http://rivet.hepforge.org/>)."] This information is

taken from the ATLAS Data Access Policy, which is a public document that can be downloaded from <http://opendata.cern.ch/record/413> [opendata.cern.ch].]

Open Access This article is licensed under a Creative Commons Attribution 4.0 International License, which permits use, sharing, adaptation, distribution and reproduction in any medium or format, as long as you give appropriate credit to the original author(s) and the source, provide a link to the Creative Commons licence, and indicate if changes were made. The images or other third party material in this article are included in the article's Creative Commons licence, unless indicated otherwise in a credit line to the material. If material is not included in the article's Creative Commons licence and your intended use is not permitted by statutory regulation or exceeds the permitted use, you will need to obtain permission directly from the copyright holder. To view a copy of this licence, visit <http://creativecommons.org/licenses/by/4.0/>.

Funded by SCOAP³.

References

1. N. Arkani-Hamed, N. Weiner, LHC signals for a superunified theory of dark matter. *JHEP* **12**, 104 (2008). [arXiv:0810.0714](https://arxiv.org/abs/0810.0714) [hep-ph]
2. M. Baumgart, C. Cheung, J.T. Ruderman, L.-T. Wang, I. Yavin, Non-abelian dark sectors and their collider signatures. *JHEP* **04**, 014 (2009). [arXiv:0901.0283](https://arxiv.org/abs/0901.0283) [hep-ph]
3. A. Falkowski, R. Vega-Morales, Exotic Higgs decays in the golden channel. *JHEP* **12**, 037 (2014). [arXiv:1405.1095](https://arxiv.org/abs/1405.1095) [hep-ph]
4. D. Curtin, R. Essig, S. Gori, J. Shelton, Illuminating dark photons with high-energy colliders. *JHEP* **02**, 157 (2015). [arXiv:1412.0018](https://arxiv.org/abs/1412.0018) [hep-ph]
5. C. Cheung, J.T. Ruderman, L.-T. Wang, I. Yavin, Lepton jets in (supersymmetric) electroweak processes. *JHEP* **04**, 116 (2010). [arXiv:0909.0290](https://arxiv.org/abs/0909.0290) [hep-ph]
6. A. Falkowski, J.T. Ruderman, T. Volansky, J. Zupan, Hidden Higgs decaying to lepton jets. *JHEP* **05**, 077 (2010). [arXiv:1002.2952](https://arxiv.org/abs/1002.2952) [hep-ph]
7. A. Falkowski, J.T. Ruderman, T. Volansky, J. Zupan, Discovering Higgs boson decays to lepton jets at hadron colliders. *Phys. Rev. Lett.* **105**, 241801 (2010). [arXiv:1007.3496](https://arxiv.org/abs/1007.3496) [hep-ph]
8. ATLAS Collaboration, A detailed map of Higgs boson interactions by the ATLAS experiment ten years after the discovery. *Nature* **607**, 52 (2022). [arXiv:2207.00092](https://arxiv.org/abs/2207.00092) [hep-ex]
9. C. Cheung, J.T. Ruderman, L.-T. Wang, I. Yavin, Kinetic mixing as the origin of a light dark-gauge-group scale. *Phys. Rev. D* **80**, 035008 (2009). [arXiv:0902.3246](https://arxiv.org/abs/0902.3246) [hep-ph]
10. B. Batell, M. Pospelov, A. Ritz, Probing a secluded U(1) at B factories. *Phys. Rev. D* **79**, 115008 (2009). [arXiv:0903.0363](https://arxiv.org/abs/0903.0363) [hep-ph]
11. P. Meade, M. Papucci, T. Volansky, Dark matter sees the light. *JHEP* **12**, 052 (2009). [arXiv:0901.2925](https://arxiv.org/abs/0901.2925) [hep-ph]
12. Particle Data Group, P. Zyla et al., Review of particle physics. *PTEP* **2020**, 083C01 (2020)
13. M.J. Strassler, K.M. Zurek, Echoes of a hidden valley at hadron colliders. *Phys. Lett. B* **651**, 374 (2007). [arXiv:hep-ph/0604261](https://arxiv.org/abs/hep-ph/0604261)
14. ATLAS Collaboration, Search for displaced muonic lepton jets from light Higgs boson decay in proton-proton collisions at $\sqrt{s} = 7$ TeV with the ATLAS detector. *Phys. Lett. B* **721**, 32(2013). [arXiv:1210.0435](https://arxiv.org/abs/1210.0435) [hep-ex]
15. ATLAS Collaboration, Search for long-lived neutral particles decaying into lepton jets in proton-proton collisions at $\sqrt{s} = 8$ TeV with the ATLAS detector. *JHEP* **11**, 088 (2014). [arXiv:1409.0746](https://arxiv.org/abs/1409.0746) [hep-ex]

16. ATLAS Collaboration, v Search for light long-lived neutral particles produced in pp collisions at $\sqrt{s} = 13$ TeV and decaying into collimated leptons or light hadrons with the ATLAS detector. *Eur. Phys. J. C* **80**, 450 (2020). [arXiv:1909.01246](#) [hep-ex]
17. ATLAS Collaboration, Search for light long-lived neutral particles that decay to collimated pairs of leptons or light hadrons in pp collisions at $\sqrt{s} = 13$ TeV with the ATLAS detector. *JHEP* **06**, 153 (2022). [arXiv:2206.12181](#) [hep-ex]
18. ATLAS Collaboration, Search for WH production with a light Higgs boson decaying to prompt electron-jets in proton-proton collisions at $\sqrt{s} = 7$ TeV with the ATLAS detector. *New J. Phys.* **15**, 043009 (2013). [arXiv:1302.4403](#) [hep-ex]
19. ATLAS Collaboration, vA search for prompt lepton-jets in pp collisions at $\sqrt{s} = 7$ TeV with the ATLAS detector. *Phys. Lett. B* **719**, 299 (2013). [arXiv:1212.5409](#) [hep-ex]
20. ATLAS Collaboration, vA search for prompt lepton-jets in pp collisions at $\sqrt{s} = 8$ TeV with the ATLAS detector. *JHEP* **02**, 062 (2016). [arXiv:1511.05542](#) [hep-ex]
21. ATLAS Collaboration, Search for long-lived particles in final states with displaced dimuon vertices in pp collisions at $\sqrt{s} = 13$ TeV with the ATLAS detector. *Phys. Rev. D* **99**, 012001 (2019). [arXiv:1808.03057](#) [hep-ex]
22. CDF Collaboration, Search for anomalous production of multiple leptons in association with W and Z bosons at CDF. *Phys. Rev. D* **85**, 092001 (2012). [arXiv:1202.1260](#) [hep-ex]
23. D0 Collaboration, Search for dark photons from supersymmetric hidden valleys. *Phys. Rev. Lett.* **103**, 081802 (2009). [arXiv:0905.1478](#) [hep-ex]
24. D0 Collaboration, Search for events with leptonic jets and missing transverse energy in $p\bar{p}$ collisions at $\sqrt{s} = 1.96$ TeV. *Phys. Rev. Lett.* **105**, 211802 (2010). [arXiv:1008.3356](#) [hep-ex]
25. CMS Collaboration, Search for light resonances decaying into pairs of muons as a signal of new physics. *JHEP* **07**, 098 (2011). [arXiv:1106.2375](#) [hep-ex]
26. CMS Collaboration, Search for a non-standard-model Higgs boson decaying to a pair of new light bosons in four-muon final states. *Phys. Lett. B* **726**, 564 (2013). [arXiv:1210.7619](#) [hep-ex]
27. CMS Collaboration, A search for pair production of new light bosons decaying into muons. *Phys. Lett. B* **752**, 146 (2016). [arXiv:1506.00424](#) [hep-ex]
28. CMS Collaboration, Search for dark photons in decays of Higgs bosons produced in association with Z bosons in proton-proton collisions at $\sqrt{s} = 13$ TeV. *JHEP* **10**, 139 (2019). [arXiv:1908.02699](#) [hep-ex]
29. LHCb Collaboration, Search for hidden-sector bosons in $B^0 \rightarrow K^{*0} \mu^+ \mu^-$ decays. *Phys. Rev. Lett.* **115**, 161802 (2015). [arXiv:1508.04094](#) [hep-ex]
30. LHCb Collaboration, Search for $A' \rightarrow \mu^+ \mu^-$ decays. *Phys. Rev. Lett.* **124**, 041801 (2020). [arXiv:1910.06926](#) [hep-ex]
31. J. Blümlein, J. Brunner, New exclusion limits for dark gauge forces from beam-dump data. *Phys. Lett. B* **701**, 155 (2011). [arXiv:1104.2747](#) [hep-ex]
32. J.D. Bjorken, R. Essig, P. Schuster, N. Toro, New fixed-target experiments to search for dark gauge forces. *Phys. Rev. D* **80**, 075018 (2009). [arXiv:0906.0580](#) [hep-ph]
33. A. Bross et al., Search for short-lived particles produced in an electron beam dump. *Phys. Rev. Lett.* **67**, 2942 (1991)
34. A1 Collaboration, Search for light gauge bosons of the dark sector at the Mainz microtron. *Phys. Rev. Lett.* **106**, 251802 (2011). [arXiv:1101.4091](#) [nucl-ex]
35. WASA-at-COSY Collaboration, Search for a dark photon in the $\pi^0 \rightarrow e^+ e^- \gamma$ decay. *Phys. Lett. B* **726**, 187 (2013). [arXiv:1304.0671](#) [hep-ex]
36. S. Abrahamyan et al., Search for a new gauge boson in electron-nucleus fixed-target scattering by the APEX experiment. *Phys. Rev. Lett.* **107**, 191804 (2011). [arXiv:1108.2750](#) [hep-ex]
37. M. Reece, L.-T. Wang, Searching for the light dark gauge boson in GeV-scale experiments. *JHEP* **07**, 051 (2009). [arXiv:0904.1743](#) [hep-ph]
38. J. Blümlein, J. Brunner, New exclusion limits on dark gauge forces from proton Bremsstrahlung in beam-dump data. *Phys. Lett. B* **731**, 320 (2014). [arXiv:1311.3870](#) [hep-ph]
39. S.N. Gninenko, Constraints on sub-GeV hidden sector gauge bosons from a search for heavy neutrino decays. *Phys. Lett. B* **713**, 244 (2012). [arXiv:1204.3583](#) [hep-ph]
40. R. Essig, R. Harnik, J. Kaplan, N. Toro, Discovering new light states at neutrino experiments. *Phys. Rev. D* **82**, 113008 (2010). [arXiv:1008.0636](#) [hep-ph]
41. HADES Collaboration, Searching a dark photon with HADES. *Phys. Lett. B* **731**, 265 (2014). [arXiv:1311.0216](#) [hep-ex]
42. KLOE-2 Collaboration, Search for a vector gauge boson in ρ meson decays with the KLOE detector. *Phys. Lett. B* **706**, 251 (2012). [arXiv:1110.0411](#) [hep-ex]
43. KLOE-2 Collaboration, Limit on the production of a light vector gauge boson in ϕ meson decays with the KLOE detector. *Phys. Lett. B* **720**, 111 (2013). [arXiv:1210.3927](#) [hep-ex]
44. BABAR Collaboration, Search for dimuon decays of a light scalar boson in radiative transitions $\Upsilon \rightarrow \gamma A^0$. *Phys. Rev. Lett.* **103**, 081803 (2009). [arXiv:0905.4539](#) [hep-ex]
45. BABAR Collaboration, Search for a dark photon in e^+e^- collisions at BaBar. *Phys. Rev. Lett.* **113**, 201801 (2014). [arXiv:1406.2980](#) [hep-ex]
46. BABAR Collaboration, Search for long-lived particles in e^+e^- collisions. *Phys. Rev. Lett.* **114**, 171801 (2015). [arXiv:1502.02580](#) [hep-ex]
47. Belle Collaboration, Search for the dark photon and the dark Higgs boson at Belle. *Phys. Rev. Lett.* **114**, 211801 (2015). [arXiv:1502.00084](#) [hep-ex]
48. Belle Collaboration, Search for a dark vector gauge boson decaying to $\pi^+ \pi^-$ using $\eta \rightarrow \pi^+ \pi^- \gamma$ decays. *Phys. Rev. D* **94**, 092006 (2016). [arXiv:1609.05599](#) [hep-ex]
49. BESIII Collaboration, Measurement of $\mathcal{B}(J/\psi \rightarrow \eta' e^+ e^-)$ and search for a dark photon. *Phys. Rev. D* **99**, 012013 (2019). [arXiv:1809.00635](#) [hep-ex]
50. BESIII Collaboration, Dark photon search in the mass range between 1.5 and 3.4 GeV/c^2 . *Phys. Lett. B* **774**, 252 (2017). [arXiv:1705.04265](#) [hep-ex]
51. M. Pospelov, Secluded U(1) below the weak scale. *Phys. Rev. D* **80**, 095002 (2009). [arXiv:0811.1030](#) [hep-ph]
52. H. Davoudiasl, H.-S. Lee, W.J. Marciano, Dark side of Higgs diphoton decays and muon $g-2$. *Phys. Rev. D* **86**, 095009 (2012). [arXiv:1208.2973](#) [hep-ph]
53. M. Endo, K. Hamaguchi, G. Mishima, Constraints on hidden photon models from electron $g-2$ and hydrogen spectroscopy. *Phys. Rev. D* **86**, 095029 (2012). [arXiv:1209.2558](#) [hep-ph]
54. J.H. Chang, R. Essig, S.D. McDermott, Supernova 1987A constraints on sub-GeV dark sectors, millicharged particles, the QCD axion, and an axion-like particle. *JHEP* **09**, 051 (2018). [arXiv:1803.00993](#) [hep-ph]
55. H.K. Dreiner, J.-F. Fortin, C. Hanhart, L. Ubaldi, Supernova constraints on MeV dark sectors from e^+e^- annihilations. *Phys. Rev. D* **89**, 105015 (2014). [arXiv:1310.3826](#) [hep-ph]
56. ATLAS Collaboration, The ATLAS Experiment at the CERN Large Hadron Collider. *JINST* **3**, S08003 (2008)
57. ATLAS Collaboration, ATLAS Insertable B-Layer: Technical Design Report, ATLAS-TDR-19; CERN-LHCC-2010-013 (2010). <https://cds.cern.ch/record/1291633> [Addendum: ATLAS-TDR-19-ADD-1; CERN-LHCC-2012-009 (2012). <https://cds.cern.ch/record/1451888>]
58. B. Abbott et al., Production and integration of the ATLAS Insertable B-Layer. *JINST* **13**, T05008 (2018). [arXiv:1803.00844](#) [physics.ins-det]

59. ATLAS Collaboration, Performance of the ATLAS trigger system in 2015. *Eur. Phys. J. C* **77**, 317 (2017). [arXiv:1611.09661](https://arxiv.org/abs/1611.09661) [hep-ex]
60. ATLAS Collaboration, The ATLAS Collaboration Software and Firmware, ATL-SOFT-PUB-2021-001 (2021). <https://cds.cern.ch/record/2767187>
61. ATLAS Collaboration, ATLAS data quality operations and performance for 2015–2018 data-taking. *JINST* **15**, P04003 (2020). [arXiv:1911.04632](https://arxiv.org/abs/1911.04632) [physics.ins-det]
62. ATLAS Collaboration, Performance of the missing transverse momentum triggers for the ATLAS detector during Run-2 data taking. *JHEP* **08**, 080 (2020). [arXiv:2005.09554](https://arxiv.org/abs/2005.09554) [hep-ex]
63. ATLAS Collaboration, Triggers for displaced decays of long-lived neutral particles in the ATLAS detector. *JINST* **8**, P07015 (2013). [arXiv:1305.2284](https://arxiv.org/abs/1305.2284) [hep-ex]
64. L. Evans, P. Bryant, L.H.C. Machine, *JINST* **3**, S08001 (2008)
65. ATLAS Collaboration, Characterisation and mitigation of beam-induced backgrounds observed in the ATLAS detector during the 2011 proton-proton run. *JINST* **8**, P07004 (2013). [arXiv:1303.0223](https://arxiv.org/abs/1303.0223) [hep-ex]
66. J. Alwall et al., The automated computation of tree-level and next-to-leading order differential cross sections, and their matching to parton shower simulations. *JHEP* **07**, 079 (2014). [arXiv:1405.0301](https://arxiv.org/abs/1405.0301) [hep-ph]
67. T. Sjöstrand, S. Mrenna, P. Skands, A brief introduction to PYTHIA 8.1. *Comput. Phys. Commun.* **178**, 852 (2008). [arXiv:0710.3820](https://arxiv.org/abs/0710.3820) [hep-ph]
68. NNPDF Collaboration, R.D. Ball et al., Parton distributions with LHC data. *Nucl. Phys. B* **867**, 244 (2013). [arXiv:1207.1303](https://arxiv.org/abs/1207.1303) [hep-ph]
69. M. Cepeda et al., Higgs Physics at the HL-LHC and HE-LHC, CERN Yellow Rep. Monogr., vol. 7, p. 221, ed. by A. Dainese et al. (2019). [arXiv:1902.00134](https://arxiv.org/abs/1902.00134) [hep-ph]
70. ATLAS Collaboration, Constraining the dark sector with the monojet signature in the ATLAS experiment, ATL-PHYS-PUB-2021-020 (2021). <https://cds.cern.ch/record/2772627>
71. T. Sjöstrand et al., An introduction to PYTHIA 8.2. *Comput. Phys. Commun.* **191**, 159 (2015). [arXiv:1410.3012](https://arxiv.org/abs/1410.3012) [hep-ph]
72. T. Gleisberg et al., Event generation with SHERPA 1.1. *JHEP* **02**, 007 (2009). [arXiv:0811.4622](https://arxiv.org/abs/0811.4622) [hep-ph]
73. The NNPDF Collaboration, R.D. Ball et al., Parton distributions for the LHC run II. *JHEP* **04**, 040 (2015). [arXiv:1410.8849](https://arxiv.org/abs/1410.8849) [hep-ph]
74. S. Frixione, P. Nason, C. Oleari, Matching NLO QCD computations with parton shower simulations: the POWHEG method. *JHEP* **11**, 070 (2007). [arXiv:0709.2092](https://arxiv.org/abs/0709.2092) [hep-ph]
75. ATLAS Collaboration, ATLAS Pythia 8 tunes to 7 TeV data, ATL-PHYS-PUB-2014-021 (2014). <https://cds.cern.ch/record/1966419>
76. P. Golonka, Z. Was, PHOTOS Monte Carlo: a precision tool for QED corrections in Z and W decays. *Eur. Phys. J. C* **45**, 97 (2006). [arXiv:hep-ph/0506026](https://arxiv.org/abs/hep-ph/0506026)
77. J. Gao et al., CT10 next-to-next-to-leading order global analysis of QCD. *Phys. Rev. D* **89**, 033009 (2014). [arXiv:1302.6246](https://arxiv.org/abs/1302.6246) [hep-ph]
78. J. Pumplin et al., New generation of parton distributions with uncertainties from global QCD analysis. *JHEP* **07**, 012 (2002). [arXiv:hep-ph/0201195](https://arxiv.org/abs/hep-ph/0201195)
79. ATLAS Collaboration, The ATLAS Simulation Infrastructure. *Eur. Phys. J. C* **70**, 823 (2010). [arXiv:1005.4568](https://arxiv.org/abs/1005.4568) [physics.ins-det]
80. S. Agostinelli et al., GEANT4—a simulation toolkit. *Nucl. Instrum. Meth. A* **506**, 250 (2003)
81. ATLAS Collaboration, The Pythia 8 A3 tune description of ATLAS minimum bias and inelastic measurements incorporating the Donnachie–Landshoff diffractive model, ATL-PHYS-PUB-2016-017 (2016). <https://cds.cern.ch/record/2206965>
82. ATLAS Collaboration, Vertex reconstruction performance of the ATLAS detector at $\sqrt{s} = 13$ TeV, ATL-PHYS-PUB-2015-026 (2015). <https://cds.cern.ch/record/2037717>
83. ATLAS Collaboration, Properties of jets and inputs to jet reconstruction and calibration with the ATLAS detector using proton-proton collisions at $\sqrt{s} = 13$ TeV, ATL-PHYS-PUB-2015-036 (2015). <https://cds.cern.ch/record/2044564>
84. M. Cacciari, G.P. Salam, G. Soyez, The anti- k_t jet clustering algorithm. *JHEP* **04**, 063 (2008). [arXiv:0802.1189](https://arxiv.org/abs/0802.1189) [hep-ph]
85. M. Cacciari, G.P. Salam, G. Soyez, FastJet user manual. *Eur. Phys. J. C* **72**, 1896 (2012). [arXiv:1111.6097](https://arxiv.org/abs/1111.6097) [hep-ph]
86. ATLAS Collaboration, Jet energy scale measurements and their systematic uncertainties in proton-proton collisions at $\sqrt{s} = 13$ TeV with the ATLAS detector. *Phys. Rev. D* **96**, 072002 (2017). [arXiv:1703.09665](https://arxiv.org/abs/1703.09665) [hep-ex]
87. ATLAS Collaboration, Selection of jets produced in 13 TeV proton-proton collisions with the ATLAS detector, ATLAS-CONF-2015-029 (2015). <https://cds.cern.ch/record/2037702>
88. ATLAS Collaboration, Optimisation and performance studies of the ATLAS b -tagging algorithms for the 2017-18 LHC run, ATL-PHYS-PUB-2017-013 (2017). <https://cds.cern.ch/record/2273281>
89. ATLAS Collaboration, ATLAS b -jet identification performance and efficiency measurement with $t\bar{t}$ events in pp collisions at $\sqrt{s} = 13$ TeV. *Eur. Phys. J. C* **79**, 970 (2019). [arXiv:1907.05120](https://arxiv.org/abs/1907.05120) [hep-ex]
90. ATLAS Collaboration, Electron and photon performance measurements with the ATLAS detector using the 2015–2017 LHC proton-proton collision data. *JINST* **14**, P12006 (2019). [arXiv:1908.00005](https://arxiv.org/abs/1908.00005) [hep-ex]
91. ATLAS Collaboration, Muon reconstruction and identification efficiency in ATLAS using the full Run 2 pp collision data set at $\sqrt{s} = 13$ TeV. *Eur. Phys. J. C* **81**, 578 (2021). [arXiv:2012.00578](https://arxiv.org/abs/2012.00578) [hep-ex]
92. ATLAS Collaboration, Performance of missing transverse momentum reconstruction with the ATLAS detector in the first proton-proton collisions at $\sqrt{s} = 13$ TeV, ATL-PHYS-PUB-2015-027 (2015). <https://cds.cern.ch/record/2037904>
93. ATLAS Collaboration, E_T^{miss} performance in the ATLAS detector using 2015–2016 LHC pp collisions, ATLAS-CONF-2018-023 (2018). <https://cds.cern.ch/record/2625233>
94. Y.L. Dokshitzer, G.D. Leder, S. Moretti, B.R. Webber, Better jet clustering algorithms. *JHEP* **08**, 001 (1997). [arXiv:hep-ph/9707323](https://arxiv.org/abs/hep-ph/9707323) [hep-ph]
95. M. Abadi et al., TensorFlow: Large-Scale Machine Learning on Heterogeneous Distributed Systems (2016). [arXiv:1603.04467](https://arxiv.org/abs/1603.04467) [cs.DC]
96. ATLAS Collaboration, Performance of pile-up mitigation techniques for jets in pp collisions at $\sqrt{s} = 8$ TeV using the ATLAS detector. *Eur. Phys. J. C* **76**, 581 (2016). [arXiv:1510.03823](https://arxiv.org/abs/1510.03823) [hep-ex]
97. ATLAS Collaboration, Monitoring and data quality assessment of the ATLAS liquid argon calorimeter. *JINST* **9**, P07024 (2014). [arXiv:1405.3768](https://arxiv.org/abs/1405.3768) [hep-ex]
98. ATLAS Collaboration, Topological cell clustering in the ATLAS calorimeters and its performance in LHC Run 1. *Eur. Phys. J. C* **77**, 490 (2017). [arXiv:1603.02934](https://arxiv.org/abs/1603.02934) [hep-ex]
99. ATLAS Collaboration, Measurement of the inelastic proton-proton cross section at $\sqrt{s} = 13$ TeV with the ATLAS detector at the LHC. *Phys. Rev. Lett.* **117**, 182002 (2016). [arXiv:1606.02625](https://arxiv.org/abs/1606.02625) [hep-ex]
100. ATLAS Collaboration, ν Luminosity determination in pp collisions at $\sqrt{s} = 13$ TeV using the ATLAS detector at the LHC, ATLAS-CONF-2019-021 (2019). <https://cds.cern.ch/record/2677054>

101. G. Avoni et al., The new LUCID-2 detector for luminosity measurement and monitoring in ATLAS. *JINST* **13**, P07017 (2018)
102. A.L. Read, Presentation of search results: the CL_S technique. *J. Phys. G* **28**, 2693 (2002)
103. G. Cowan, K. Cranmer, E. Gross, O. Vitells, Asymptotic formulae for likelihood-based tests of new physics. *Eur. Phys. J. C* **71**, 1554 (2011). [arXiv:1007.1727](https://arxiv.org/abs/1007.1727) [physics.data-an] [Erratum: *Eur. Phys. J. C* **73** (2013) 2501]
104. ATLAS Collaboration, ATLAS Computing Acknowledgements, ATL-SOFT-PUB-2023-001 (2023). <https://cds.cern.ch/record/2869272>

ATLAS Collaboration*

G. Aad¹⁰², B. Abbott¹²⁰, K. Abeling⁵⁵, N. J. Abicht⁴⁹, S. H. Abidi²⁹, A. Aboulhorma^{35e}, H. Abramowicz¹⁵¹, H. Abreu¹⁵⁰, Y. Abulaiti¹¹⁷, B. S. Acharya^{69a,69b,m}, C. Adam Bourdarios⁴, L. Adamczyk^{86a}, S. V. Addepalli²⁶, M. J. Addison¹⁰¹, J. Adelman¹¹⁵, A. Adiguzel^{21c}, T. Auyeub¹³⁴, A. A. Affolder¹³⁶, Y. Afik³⁶, M. N. Agaras¹³, J. Agarwala^{73a,73b}, A. Aggarwal¹⁰⁰, C. Agheorghiesei^{27c}, A. Ahmad³⁶, F. Ahmadov^{38,y}, W. S. Ahmed¹⁰⁴, S. Ahuja⁹⁵, X. Ai^{62a}, G. Aielli^{76a,76b}, A. Aikot¹⁶³, M. Ait Tamlihat^{35e}, B. Aitbenkhik^{35a}, I. Aizenberg¹⁶⁹, M. Akbiyik¹⁰⁰, T. P. A. Åkesson⁹⁸, A. V. Akimov³⁷, D. Akiyama¹⁶⁸, N. N. Akolkar²⁴, S. Aktas^{21a}, K. Al Khoury⁴¹, G. L. Alberghi^{23b}, J. Albert¹⁶⁵, P. Albicocco⁵³, G. L. Albouy⁶⁰, S. Alderweireldt⁵², Z. L. Alegria¹²¹, M. Aleksa³⁶, I. N. Aleksandrov³⁸, C. Alexa^{27b}, T. Alexopoulos¹⁰, F. Alfonsi^{23b}, M. Algren⁵⁶, M. Alhroob¹²⁰, B. Ali¹³², H. M. J. Ali⁹¹, S. Ali¹⁴⁸, S. W. Alibocus⁹², M. Aliev¹⁴⁵, G. Alimonti^{71a}, W. Alkakh⁵⁵, C. Allaire⁶⁶, B. M. M. Allbrooke¹⁴⁶, J. F. Allen⁵², C. A. Allendes Flores^{137f}, P. P. Allport²⁰, A. Aloisio^{72a,72b}, F. Alonso⁹⁰, C. Alpighiani¹³⁸, M. Alvarez Estevez⁹⁹, A. Alvarez Fernandez¹⁰⁰, M. Alves Cardoso⁵⁶, M. G. Alvigi^{72a,72b}, M. Aly¹⁰¹, Y. Amaral Coutinho^{83b}, A. Ambler¹⁰⁴, C. Amelung³⁶, M. Ameri¹⁰¹, C. G. Ames¹⁰⁹, D. Amidei¹⁰⁶, S. P. Amor Dos Santos^{130a}, K. R. Amos¹⁶³, V. Ananiev¹²⁵, C. Anastopoulos¹³⁹, T. Andeen¹¹, J. K. Anders³⁶, S. Y. Andrean^{47a,47b}, A. Andreazza^{71a,71b}, S. Angelidakis⁹, A. Angerami^{41,ab}, A. V. Anisenkov³⁷, A. Annovi^{74a}, C. Antel⁵⁶, M. T. Anthony¹³⁹, E. Antipov¹⁴⁵, M. Antonelli⁵³, F. Anulli^{75a}, M. Aoki⁸⁴, T. Aoki¹⁵³, J. A. Aparisi Pozo¹⁶³, M. A. Aparo¹⁴⁶, L. Aperio Bella⁴⁸, C. Appelt¹⁸, A. Apyan²⁶, N. Aranzabal³⁶, S. J. Arbiol Val⁸⁷, C. Arcangeletti⁵³, A. T. H. Arce⁵¹, E. Arena⁹², J-F. Arguin¹⁰⁸, S. Argyropoulos⁵⁴, J.-H. Arling⁴⁸, O. Arnaez⁴, H. Arnold¹¹⁴, G. Artoni^{75a,75b}, H. Asada¹¹¹, K. Asai¹¹⁸, S. Asai¹⁵³, N. A. Asbah⁶¹, K. Assamagan²⁹, R. Astalos^{28a}, S. Atashi¹⁶⁰, R. J. Atkin^{33a}, M. Atkinson¹⁶², H. Atmani^{35f}, P. A. Atlasidha¹²⁸, K. Augsten¹³², S. Auricchio^{72a,72b}, A. D. Auriol²⁰, V. A. Austrup¹⁰¹, G. Avolio³⁶, K. Axiotis⁵⁶, G. Azuelos^{108,af}, D. Babal^{28b}, H. Bachacou¹³⁵, K. Bachas^{152,p}, A. Bachi³⁴, F. Backman^{47a,47b}, A. Badea⁶¹, T. M. Baer¹⁰⁶, P. Bagnaia^{75a,75b}, M. Bahmani¹⁸, D. Bahner⁵⁴, A. J. Bailey¹⁶³, V. R. Bailey¹⁶², J. T. Baines¹³⁴, L. Baines⁹⁴, O. K. Baker¹⁷², E. Bakos¹⁵, D. Bakshi Gupta⁸, V. Balakrishnan¹²⁰, R. Balasubramanian¹¹⁴, E. M. Baldin³⁷, P. Balek^{86a}, E. Ballabene^{23a,23b}, F. Balli¹³⁵, L. M. Baltes^{63a}, W. K. Balunas³², J. Balz¹⁰⁰, E. Banas⁸⁷, M. Bandieramonte¹²⁹, A. Bandyopadhyay²⁴, S. Bansal²⁴, L. Barak¹⁵¹, M. Barakat⁴⁸, E. L. Barberio¹⁰⁵, D. Barberis^{57a,57b}, M. Barbero¹⁰², M. Z. Barel¹¹⁴, K. N. Barends^{33a}, T. Barillari¹¹⁰, M.-S. Barisits³⁶, T. Barklow¹⁴³, P. Baron¹²², D. A. Baron Moreno¹⁰¹, A. Baroncelli^{62a}, G. Barone²⁹, A. J. Barr¹²⁶, J. D. Barr⁹⁶, L. Barranco Navarro^{47a,47b}, F. Barreiro⁹⁹, J. Barreiro Guimarães da Costa^{14a}, U. Barron¹⁵¹, M. G. Barros Teixeira^{130a}, S. Barsov³⁷, F. Bartels^{63a}, R. Bartoldus¹⁴³, A. E. Barton⁹¹, P. Bartos^{28a}, A. Basan¹⁰⁰, M. Baselga⁴⁹, A. Bassalat^{66,b}, M. J. Basso^{156a}, C. R. Basson¹⁰¹, R. L. Bates⁵⁹, S. Batlamous^{35e}, J. R. Batley³², B. Batool¹⁴¹, M. Battaglia¹³⁶, D. Battulga¹⁸, M. Bause^{75a,75b}, M. Bauer³⁶, P. Bauer²⁴, L. T. Bazzano Hurrell³⁰, J. B. Beacham⁵¹, T. Beau¹²⁷, J. Y. Beauchamp⁹⁰, P. H. Beauchemin¹⁵⁸, F. Becherer⁵⁴, P. Bechtel²⁴, H. P. Beck^{19,o}, K. Becker¹⁶⁷, A. J. Beddall⁸², V. A. Bednyakov³⁸, C. P. Bee¹⁴⁵, L. J. Beemster¹⁵, T. A. Beermann³⁶, M. Begalli^{83d}, M. Beggel²⁹, A. Behara¹⁴⁵, J. K. Behr⁴⁸, J. F. Beirer³⁶, F. Beisiegel²⁴, M. Belfkir¹⁵⁹, G. Bella¹⁵¹, L. Bellagamba^{23b}, A. Bellerive³⁴, P. Bellos²⁰, K. Beloborodov³⁷, D. Benckekroun^{35a}, F. Bendebba^{35a}, Y. Benhammou¹⁵¹, M. Benoit²⁹, J. R. Bensinger²⁶, S. Bentvelsen¹¹⁴, L. Beresford⁴⁸, M. Beretta⁵³, E. Bergeas Kuutmann¹⁶¹, N. Berger⁴, B. Bergmann¹³², J. Beringer^{17a}, G. Bernardi⁵, C. Bernius¹⁴³, F. U. Bernlochner²⁴, F. Bernon^{36,102}, A. Berrocal Guardia¹³, T. Berry⁹⁵, P. Berta¹³³, A. Berthold⁵⁰, I. A. Bertram⁹¹, S. Bethke¹¹⁰, A. Betti^{75a,75b}, A. J. Bevan⁹⁴, N. K. Bhalla⁵⁴, M. Bhamjee^{33c}, S. Bhatta¹⁴⁵, D. S. Bhattacharya¹⁶⁶, P. Bhattarai¹⁴³, V. S. Bhopatkar¹²¹, R. Bi^{29,ai}, R. M. Bianchi¹²⁹, G. Bianco^{23a,23b}, O. Biebel¹⁰⁹, R. Bielski¹²³, M. Biglietti^{77a}, M. Bindi⁵⁵, A. Bingul^{21b}, C. Bini^{75a,75b}, A. Biondini⁹², C. J. Birch-sykes¹⁰¹, G. A. Bird^{20,134}, M. Birman¹⁶⁹, M. Biros¹³³, S. Biryukov¹⁴⁶, T. Bisanz⁴⁹

E. Bisceglie^{43a,43b}, J. P. Biswal¹³⁴, D. Biswas¹⁴¹, A. Bitadze¹⁰¹, K. Bjørke¹²⁵, I. Bloch⁴⁸, A. Blue⁵⁹, U. Blumenschein⁹⁴, J. Blumenthal¹⁰⁰, G. J. Bobbink¹¹⁴, V. S. Bobrovnikov³⁷, M. Boehler⁵⁴, B. Boehm¹⁶⁶, D. Bogavac³⁶, A. G. Bogdanchikov³⁷, C. Bohm^{47a}, V. Boisvert⁹⁵, P. Bokan⁴⁸, T. Bold^{86a}, M. Bomben⁵, M. Bona⁹⁴, M. Boonekamp¹³⁵, C. D. Booth⁹⁵, A. G. Borbély⁵⁹, I. S. Bordulev³⁷, H. M. Borecka-Bielska¹⁰⁸, G. Borissov⁹¹, D. Bortoletto¹²⁶, D. Boscherini^{23b}, M. Bosman¹³, J. D. Bossio Sola³⁶, K. Bouaouda^{35a}, N. Bouchhar¹⁶³, J. Boudreau¹²⁹, E. V. Bouhova-Thacker⁹¹, D. Boumediene⁴⁰, R. Bouquet¹⁶⁵, A. Boveia¹¹⁹, J. Boyd³⁶, D. Boye²⁹, I. R. Boyko³⁸, J. Bracini²⁰, N. Brahimi^{62d}, G. Brandt¹⁷¹, O. Brandt³², F. Braren⁴⁸, B. Brau¹⁰³, J. E. Brau¹²³, R. Brenner¹⁶⁹, L. Brenner¹¹⁴, R. Brenner¹⁶¹, S. Bressler¹⁶⁹, D. Britton⁵⁹, D. Britzger¹¹⁰, I. Brock²⁴, G. Brooijmans⁴¹, W. K. Brooks^{137f}, E. Brost²⁹, L. M. Brown¹⁶⁵, L. E. Bruce⁶¹, T. L. Bruckler¹²⁶, P. A. Bruckman de Renstrom⁸⁷, B. Brüers⁴⁸, A. Bruni^{23b}, G. Bruni^{23b}, M. Bruschi^{23b}, N. Bruscino^{75a,75b}, T. Buanes¹⁶, Q. Buat¹³⁸, D. Buchin¹¹⁰, A. G. Buckley⁵⁹, O. Bulekov³⁷, B. A. Bullard¹⁴³, S. Burdin⁹², C. D. Burgard⁴⁹, A. M. Burger⁴⁰, B. Burghgrave⁸, O. Burlayenko⁵⁴, J. T. P. Burr³², C. D. Burton¹¹, J. C. Burzynski¹⁴², E. L. Busch⁴¹, V. Büscher¹⁰⁰, P. J. Bussey⁵⁹, J. M. Butler²⁵, C. M. Buttar⁵⁹, J. M. Butterworth⁹⁶, W. Buttinger¹³⁴, C. J. Buxo Vazquez¹⁰⁷, A. R. Buzzykaev³⁷, S. Cabrera Urbán¹⁶³, L. Cadamuro⁶⁶, D. Caforio⁵⁸, H. Cai¹²⁹, Y. Cai^{14a,14e}, Y. Cai^{14c}, V. M. M. Cairo³⁶, O. Cakir^{3a}, N. Calace³⁶, P. Calafiura^{17a}, G. Calderini¹²⁷, P. Calfayan⁶⁸, G. Callea⁵⁹, L. P. Caloba^{83b}, D. Calvet⁴⁰, S. Calvet⁴⁰, T. P. Calvet¹⁰², M. Calvetti^{74a,74b}, R. Camacho Toro¹²⁷, S. Camarda³⁶, D. Camarero Munoz²⁶, P. Camarri^{76a,76b}, M. T. Camerlingo^{72a,72b}, D. Cameron³⁶, C. Camincher¹⁶⁵, M. Campanelli⁹⁶, A. Camplani⁴², V. Canale^{72a,72b}, A. Canesse¹⁰⁴, J. Cantero¹⁶³, Y. Cao¹⁶², F. Capocasa²⁶, M. Capua^{43a,43b}, A. Carbone^{71a,71b}, R. Cardarelli^{76a}, J. C. J. Cardenas⁸, F. Cardillo¹⁶³, G. Carducci^{43a,43b}, T. Carli³⁶, G. Carlino^{72a}, J. I. Carlotto¹³, B. T. Carlson^{129,q}, E. M. Carlson^{156a,165}, L. Carminati^{71a,71b}, A. Carnelli¹³⁵, M. Carnesale^{75a,75b}, S. Caron¹¹³, E. Carquin^{137f}, S. Carrà^{71a}, G. Carratta^{23a,23b}, F. Carri Argos^{33g}, J. W. S. Carter¹⁵⁵, T. M. Carter⁵², M. P. Casado^{13,i}, M. Caspar⁴⁸, F. L. Castillo⁴, L. Castillo Garcia¹³, V. Castillo Gimenez¹⁶³, N. F. Castro^{130a,130e}, A. Catinaccio³⁶, J. R. Catmore¹²⁵, V. Cavaliere²⁹, N. Cavalli^{23a,23b}, V. Cavasinni^{74a,74b}, Y. C. Cekmecelioglu⁴⁸, E. Celebi^{21a}, F. Celli¹²⁶, M. S. Centonze^{70a,70b}, V. Cepaitis⁵⁶, K. Cerny¹²², A. S. Cerqueira^{83a}, A. Cerri¹⁴⁶, L. Cerrito^{76a,76b}, F. Cerutti^{17a}, B. Cervato¹⁴¹, A. Cervelli^{23b}, G. Cesarini⁵³, S. A. Cetin⁸², D. Chakraborty¹¹⁵, J. Chan¹⁷⁰, W. Y. Chan¹⁵³, J. D. Chapman³², E. Chapon¹³⁵, B. Chargeishvili^{149b}, D. G. Charlton²⁰, M. Chatterjee¹⁹, C. Chauhan¹³³, S. Chekanov⁶, S. V. Chekulaev^{156a}, G. A. Chelkov^{38,a}, A. Chen¹⁰⁶, B. Chen¹⁵¹, B. Chen¹⁶⁵, H. Chen^{14c}, H. Chen²⁹, J. Chen^{62c}, J. Chen¹⁴², M. Chen¹²⁶, S. Chen¹⁵³, S. J. Chen^{14c}, X. Chen^{62c,135}, X. Chen^{14b,ae}, Y. Chen^{62a}, C. L. Cheng¹⁷⁰, H. C. Cheng^{64a}, S. Cheong¹⁴³, A. Cheplakov³⁸, E. Cheremushkina⁴⁸, E. Cherepanova¹¹⁴, R. Cherkaoui El Moursli^{35e}, E. Cheu⁷, K. Cheung⁶⁵, L. Chevalier¹³⁵, V. Chiarella⁵³, G. Chiarelli^{74a}, N. Chiedde¹⁰², G. Chiodini^{70a}, A. S. Chisholm²⁰, A. Chitan^{27b}, M. Chitishvili¹⁶³, M. V. Chizhov³⁸, K. Choi¹¹, A. R. Chomont^{75a,75b}, Y. Chou¹⁰³, E. Y. S. Chow¹¹³, T. Chowdhury^{33g}, K. L. Chu¹⁶⁹, M. C. Chu^{64a}, X. Chu^{14a,14e}, J. Chudoba¹³¹, J. J. Chwastowski⁸⁷, D. Cieri¹¹⁰, K. M. Ciesla^{86a}, V. Cindro⁹³, A. Ciocio^{17a}, F. Ciroto^{72a,72b}, Z. H. Citron^{169,k}, M. Citterio^{71a}, D. A. Ciubotaru^{27b}, A. Clark⁵⁶, P. J. Clark⁵², C. Clarry¹⁵⁵, J. M. Clavijo Columbie⁴⁸, S. E. Clawson⁴⁸, C. Clement^{47a,47b}, J. Clercx⁴⁸, Y. Coadou¹⁰², M. Cobl^{69a,69c}, A. Coccaro^{57b}, R. F. Coelho Barrue^{130a}, R. Coelho Lopes De Sa¹⁰³, S. Coelli^{71a}, A. E. C. Coimbra^{71a,71b}, B. Cole⁴¹, J. Collot⁶⁰, P. Conde Muñio^{130a,130g}, M. P. Connell^{33c}, S. H. Connell^{33c}, I. A. Connelly⁵⁹, E. I. Conroy¹²⁶, F. Conventi^{72a,ag}, H. G. Cooke²⁰, A. M. Cooper-Sarkar¹²⁶, A. Cordeiro Oudot Choi¹²⁷, L. D. Corpe⁴⁰, M. Corradi^{75a,75b}, F. Corriveau^{104,w}, A. Cortes-Gonzalez¹⁸, M. J. Costa¹⁶³, F. Costanza⁴, D. Costanzo¹³⁹, B. M. Cote¹¹⁹, G. Cowan⁹⁵, K. Cranmer¹⁷⁰, D. Cremonini^{23a,23b}, S. Crépe-Renaudin⁶⁰, F. Crescioli¹²⁷, M. Cristinziani¹⁴¹, M. Cristoforetti^{78a,78b}, V. Croft¹¹⁴, J. E. Crosby¹²¹, G. Crosetti^{43a,43b}, A. Cueto⁹⁹, T. Cuhadar Donszelmann¹⁶⁰, H. Cui^{14a,14e}, Z. Cui⁷, W. R. Cunningham⁵⁹, F. Curcio^{43a,43b}, P. Czodrowski³⁶, M. M. Czurylo^{63b}, M. J. Da Cunha Sargedas De Sousa^{57a,57b}, J. V. Da Fonseca Pinto^{83b}, C. Da Via¹⁰¹, W. Dabrowski^{86a}, T. Dado⁴⁹, S. Dahbi^{33g}, T. Dai¹⁰⁶, D. Dal Santo¹⁹, C. Dallapiccola¹⁰³, M. Dam⁴², G. D'amen²⁹, V. D'Amico¹⁰⁹, J. Damp¹⁰⁰, J. R. Dandoy³⁴, M. F. Daneri³⁰, M. Danninger¹⁴², V. Dao³⁶, G. Darbo^{57b}, S. Darmora⁶, S. J. Das^{29,ai}, S. D'Auria^{71a,71b}, C. David^{156b}, T. Davidek¹³³, B. Davis-Purcell³⁴, I. Dawson⁹⁴, H. A. Day-hall¹³², K. De⁸, R. De Asmundis^{72a}, N. De Biase⁴⁸, S. De Castro^{23a,23b}, N. De Groot¹¹³, P. de Jong¹¹⁴, H. Dela Torre¹¹⁵, A. De Maria^{14c}, A. De Salvo^{75a}, U. De Sanctis^{76a,76b}, F. De Santis^{70a,70b}, A. De Santo¹⁴⁶, J. B. De Vivie DeRegie⁶⁰, D. V. Dedovich³⁸, J. Degens¹¹⁴, A. M. Deiana⁴⁴, F. Del Corso^{23a,23b}, J. Del Peso⁹⁹, F. Del Rio^{63a}, L. Delagrange¹²⁷, F. Deliot¹³⁵, C. M. Delitzsch⁴⁹,

A. Gongadze^{149c}, F. Gonnella²⁰, J. L. Gonski⁴¹, R. Y. González Andana⁵², S. González dela Hoz¹⁶³, S. Gonzalez Fernandez¹³, R. Gonzalez Lopez⁹², C. Gonzalez Renteria^{17a}, M. V. Gonzalez Rodrigues⁴⁸, R. Gonzalez Suarez¹⁶¹, S. Gonzalez-Sevilla⁵⁶, G. R. Gonzalvo Rodriguez¹⁶³, L. Goossens³⁶, B. Gorini³⁶, E. Gorini^{70a,70b}, A. Gorišek⁹³, T. C. Gosart¹²⁸, A. T. Goshaw⁵¹, M. I. Gostkin³⁸, S. Goswami¹²¹, C. A. Gottardo³⁶, S. A. Gotz¹⁰⁹, M. Goughri^{35b}, V. Goumarre⁴⁸, A. G. Goussiou¹³⁸, N. Govender^{33c}, I. Grabowska-Bold^{86a}, K. Graham³⁴, E. Gramstad¹²⁵, S. Grancagnolo^{70a,70b}, M. Grandi¹⁴⁶, C. M. Grant^{1,135}, P. M. Gravila^{27f}, F. G. Gravili^{70a,70b}, H. M. Gray^{17a}, M. Greco^{70a,70b}, C. Grefe²⁴, I. M. Gregor⁴⁸, P. Grenier¹⁴³, S. G. Grewe¹¹⁰, C. Grieco¹³, A. A. Grillo¹³⁶, K. Grimm³¹, S. Grinstein^{13,s}, J.-F. Grivaz⁶⁶, E. Gross¹⁶⁹, J. Grosse-Knetter⁵⁵, C. Grud¹⁰⁶, J. C. Grundy¹²⁶, L. Guan¹⁰⁶, W. Guan²⁹, C. Gubbels¹⁶⁴, J. G. R. Guerrero Rojas¹⁶³, G. Guerrieri^{69a,69c}, F. Guescini¹¹⁰, R. Gugel¹⁰⁰, J. A. M. Guhit¹⁰⁶, A. Guida¹⁸, E. Guillon^{134,167}, S. Guindon³⁶, F. Guo^{14a,14e}, J. Guo^{62c}, L. Guo⁴⁸, Y. Guo¹⁰⁶, R. Gupta⁴⁸, R. Gupta¹²⁹, S. Gurbuz²⁴, S. S. Gurdasani⁵⁴, G. Gustavoino³⁶, M. Guth⁵⁶, P. Gutierrez¹²⁰, L. F. Gutierrez Zagazeta¹²⁸, M. Gutsche⁵⁰, C. Gutschow⁹⁶, C. Gwenlan¹²⁶, C. B. Gwilliam⁹², E. S. Haaland¹²⁵, A. Haas¹¹⁷, M. Habedank⁴⁸, C. Haber^{17a}, H. K. Hadavand⁸, A. Hadeef⁵⁰, S. Hadzic¹¹⁰, A. I. Hagan⁹¹, J. J. Hahn¹⁴¹, E. H. Haines⁹⁶, M. Haleem¹⁶⁶, J. Haley¹²¹, J. J. Hall¹³⁹, G. D. Hallewell¹⁰², L. Halser¹⁹, K. Hamano¹⁶⁵, M. Hamer²⁴, G. N. Hamity⁵², E. J. Hampshire⁹⁵, J. Han^{62b}, K. Han^{62a}, L. Han^{14c}, L. Han^{62a}, S. Han^{17a}, Y. F. Han¹⁵⁵, K. Hanagaki⁸⁴, M. Hance¹³⁶, D. A. Hangal^{41,ab}, H. Hanif¹⁴², M. D. Hank¹²⁸, R. Hankache¹⁰¹, J. B. Hansen⁴², J. D. Hansen⁴², P. H. Hansen⁴², K. Hara¹⁵⁷, D. Harada⁵⁶, T. Harenberg¹⁷¹, S. Harkusha³⁷, M. L. Harris¹⁰³, Y. T. Harris¹²⁶, J. Harrison¹³, N. M. Harrison¹¹⁹, P. F. Harrison¹⁶⁷, N. M. Hartman¹¹⁰, N. M. Hartmann¹⁰⁹, Y. Hasegawa¹⁴⁰, R. Hauser¹⁰⁷, C. M. Hawkes²⁰, R. J. Hawkins³⁶, Y. Hayashi¹⁵³, S. Hayashida¹¹¹, D. Hayden¹⁰⁷, C. Hayes¹⁰⁶, R. L. Hayes¹¹⁴, C. P. Hays¹²⁶, J. M. Hays⁹⁴, H. S. Hayward⁹², F. He^{62a}, M. He^{14a,14e}, Y. He¹⁵⁴, Y. He⁴⁸, N. B. Heatley⁹⁴, V. Hedberg⁹⁸, A. L. Heggelund¹²⁵, N. D. Hehir^{94,*}, C. Heidegger⁵⁴, K. K. Heidegger⁵⁴, W. D. Heidorn⁸¹, J. Heilman³⁴, S. Heim⁴⁸, T. Heim^{17a}, J. G. Heinlein¹²⁸, J. J. Heinrich¹²³, L. Heinrich^{110,ad}, J. Hejbal¹³¹, L. Helary⁴⁸, A. Held¹⁷⁰, S. Hellesund¹⁶, C. M. Helling¹⁶⁴, S. Hellman^{47a,47b}, R. C. W. Henderson⁹¹, L. Henkelmann³², A. M. Henriques Correia³⁶, H. Herde⁹⁸, Y. Hernández Jiménez¹⁴⁵, L. M. Herrmann²⁴, T. Herrmann⁵⁰, G. Herten⁵⁴, R. Hertenberger¹⁰⁹, L. Hervas³⁶, M. E. Hesping¹⁰⁰, N. P. Hessey^{156a}, H. Hibi⁸⁵, E. Hill¹⁵⁵, S. J. Hillier²⁰, J. R. Hinds¹⁰⁷, F. Hinterkeuser²⁴, M. Hirose¹²⁴, S. Hirose¹⁵⁷, D. Hirschbuehl¹⁷¹, T. G. Hitchings¹⁰¹, B. Hiti⁹³, J. Hobbs¹⁴⁵, R. Hobincu^{27e}, N. Hod¹⁶⁹, M. C. Hodgkinson¹³⁹, B. H. Hodgkinson³², A. Hoecker³⁶, D. D. Hofer¹⁰⁶, J. Hofer⁴⁸, T. Holm²⁴, M. Holzbock¹¹⁰, L. B. A. H. Hommels³², B. P. Honan¹⁰¹, J. Hong^{62c}, T. M. Hong¹²⁹, B. H. Hooberman¹⁶², W. H. Hopkins⁶, Y. Horii¹¹¹, S. Hou¹⁴⁸, A. S. Howard⁹³, J. Howarth⁵⁹, J. Hoya⁶, M. Hrabovsky¹²², A. Hrynevich⁴⁸, T. Hryn'ova⁴, P. J. Hsu⁶⁵, S.-C. Hsu¹³⁸, Q. Hu^{62a}, Y. F. Hu^{14a,14e}, S. Huang^{64b}, X. Huang^{14c}, X. Huang^{14a,14e}, Y. Huang¹³⁹, Y. Huang^{14a}, Z. Huang¹⁰¹, Z. Hubacek¹³², M. Huebner²⁴, F. Huegging²⁴, T. B. Huffman¹²⁶, C. A. Hugli⁴⁸, M. Huhtinen³⁶, S. K. Huiberts¹⁶, R. Hulsken¹⁰⁴, N. Huseynov¹², J. Huston¹⁰⁷, J. Huth⁶¹, R. Hyneman¹⁴³, G. Iacobucci⁵⁶, G. Iakovidis²⁹, I. Ibragimov¹⁴¹, L. Iconomidou-Fayard⁶⁶, P. Iengo^{72a,72b}, R. Iguchi¹⁵³, T. Iizawa¹²⁶, Y. Ikegami⁸⁴, N. Ilic¹⁵⁵, H. Imam^{35a}, M. Ince Lezki⁵⁶, T. Ingebreetsen Carlson^{47a,47b}, G. Introzzi^{73a,73b}, M. Iodice^{77a}, V. Ippolito^{75a,75b}, R. K. Irwin⁹², M. Ishino¹⁵³, W. Islam¹⁷⁰, C. Issever^{18,48}, S. Istin^{21a,ak}, H. Ito¹⁶⁸, J. M. Iturbe Ponce^{64a}, R. Iuppa^{78a,78b}, A. Ivina¹⁶⁹, J. M. Izen⁴⁵, V. Izzo^{72a}, P. Jacka^{131,132}, P. Jackson¹, R. M. Jacobs⁴⁸, B. P. Jaeger¹⁴², C. S. Jagfeld¹⁰⁹, G. Jain^{156a}, P. Jain⁵⁴, K. Jakobs⁵⁴, T. Jakoubek¹⁶⁹, J. Jamieson⁵⁹, K. W. Janas^{86a}, M. Javurkova¹⁰³, F. Jeanneau¹³⁵, L. Jeanty¹²³, J. Jejelava^{149a,z}, P. Jenni^{54,g}, C. E. Jessiman³⁴, S. Jézéquel⁴, C. Jia^{62b}, J. Jia¹⁴⁵, X. Jia⁶¹, X. Jia^{14a,14c}, Z. Jia^{14c}, S. Jiggins⁴⁸, J. Jimenez Pena¹³, S. Jin^{14c}, A. Jinaru^{27b}, O. Jinnouchi¹⁵⁴, P. Johansson¹³⁹, K. A. Johns⁷, J. W. Johnson¹³⁶, D. M. Jones³², E. Jones⁴⁸, P. Jones³², R. W. L. Jones⁹¹, T. J. Jones⁹², H. L. Joos^{36,55}, R. Joshi¹¹⁹, J. Jovicevic¹⁵, X. Ju^{17a}, J. J. Junggeburth¹⁰³, T. Junkermann^{63a}, A. Juste Rozas^{13,s}, M. K. Juzek⁸⁷, S. Kabana^{137e}, A. Kaczmarska⁸⁷, M. Kado¹¹⁰, H. Kagan¹¹⁹, M. Kagan¹⁴³, A. Kahn⁴¹, A. Kahn¹²⁸, C. Kahra¹⁰⁰, T. Kaji¹⁵³, E. Kajomovitz¹⁵⁰, N. Kakati¹⁶⁹, I. Kalaitzidou⁵⁴, C. W. Kalderon²⁹, A. Kamenshchikov¹⁵⁵, N. J. Kang¹³⁶, D. Kar^{33g}, K. Karava¹²⁶, M. J. Kareem^{156b}, E. Karentzos⁵⁴, I. Karkanas¹⁵², O. Karkout¹¹⁴, S. N. Karpov³⁸, Z. M. Karpova³⁸, V. Kartvelishvili⁹¹, A. N. Karyukhin³⁷, E. Kasimi¹⁵², J. Katzy⁴⁸, S. Kaur³⁴, K. Kawade¹⁴⁰, M. P. Kawale¹²⁰, C. Kawamoto⁸⁸, T. Kawamoto^{62a}, E. F. Kay³⁶, F. I. Kaya¹⁵⁸, S. Kazakos¹⁰⁷, V. F. Kazanin³⁷, Y. Ke¹⁴⁵, J. M. Keaveney^{33a}, R. Keeler¹⁶⁵, G. V. Kehris⁶¹, J. S. Keller³⁴, A. S. Kelly⁹⁶, J. J. Kempster¹⁴⁶, K. E. Kennedy⁴¹, P. D. Kennedy¹⁰⁰, O. Kepka¹³¹, B. P. Kerridge¹⁶⁷, S. Kersten¹⁷¹, B. P. Kerševan⁹³, S. Keshri⁶⁶, L. Keszeghova^{28a}

S. Ketabchi Haghighat¹⁵⁵, R. A. Khan¹²⁹, M. Khandoga¹²⁷, A. Khanov¹²¹, A. G. Kharlamov³⁷, T. Kharlamova³⁷, E. E. Khoda¹³⁸, M. Kholodenko³⁷, T. J. Khoo¹⁸, G. Khorauli¹⁶⁶, J. Khubua^{149b}, Y. A. R. Khwairi⁶⁶, A. Kilgallon¹²³, D. W. Kim^{47a,47b}, Y. K. Kim³⁹, N. Kimura⁹⁶, M. K. Kingston⁵⁵, A. Kirchhoff⁵⁵, C. Kirfel²⁴, F. Kirfel²⁴, J. Kirk¹³⁴, A. E. Kiryunin¹¹⁰, C. Kitsaki¹⁰, O. Kivernyk²⁴, M. Klassen^{63a}, C. Klein³⁴, L. Klein¹⁶⁶, M. H. Klein¹⁰⁶, M. Klein⁹², S. B. Klein⁵⁶, U. Klein⁹², P. Klimek³⁶, A. Klimentov²⁹, T. Klioutchnikova³⁶, P. Kluit¹¹⁴, S. Kluth¹¹⁰, E. Kneringer⁷⁹, T. M. Knight¹⁵⁵, A. Knue⁴⁹, R. Kobayashi⁸⁸, D. Kobylianskii¹⁶⁹, S. F. Koch¹²⁶, M. Kocian¹⁴³, P. Kodyš¹³³, D. M. Koeck¹²³, P. T. Koenig²⁴, T. Koffas³⁴, O. Kolay⁵⁰, I. Koletsou⁴, T. Komarek¹²², K. Köneke⁵⁴, A. X. Y. Kong¹, T. Kono¹¹⁸, N. Konstantinidis⁹⁶, P. Kontaxakis⁵⁶, B. Konya⁹⁸, R. Kopeliansky⁶⁸, S. Koperny^{86a}, K. Korcyl⁸⁷, K. Kordas^{152.e}, G. Koren¹⁵¹, A. Korn⁹⁶, S. Korn⁵⁵, I. Korolkov¹³, N. Korotkova³⁷, B. Kortman¹¹⁴, O. Kortner¹¹⁰, S. Kortner¹¹⁰, W. H. Kostecka¹¹⁵, V. V. Kostyukhin¹⁴¹, A. Kotsokechagia¹³⁵, A. Kotwal⁵¹, A. Koulouris³⁶, A. Kourkouveli-Charalampidi^{73a,73b}, C. Kourkouvelis⁹, E. Kourlitis^{110.ad}, O. Kovanda¹⁴⁶, R. Kowalewski¹⁶⁵, W. Kozanecki¹³⁵, A. S. Kozhin³⁷, V. A. Kramarenko³⁷, G. Kramberger⁹³, P. Kramer¹⁰⁰, M. W. Krasny¹²⁷, A. Krasznahorkay³⁶, J. W. Kraus¹⁷¹, J. A. Kremer⁴⁸, T. Kresse⁵⁰, J. Kretzschmar⁹², K. Kreul¹⁸, P. Krieger¹⁵⁵, S. Krishnamurthy¹⁰³, M. Krivos¹³³, K. Krizka²⁰, K. Kroeninger⁴⁹, H. Kroha¹¹⁰, J. Kroll¹³¹, J. Kroll¹²⁸, K. S. Krowpman¹⁰⁷, U. Kruchonak³⁸, H. Krüger²⁴, N. Krumnack⁸¹, M. C. Kruse⁵¹, O. Kuchinskai³⁷, S. Kuday^{3a}, S. Kuehn³⁶, R. Kuesters⁵⁴, T. Kuhl⁴⁸, V. Kukhtin³⁸, Y. Kulchitsky^{37.a}, S. Kuleshov^{137b,137d}, M. Kumar^{33g}, N. Kumari⁴⁸, P. Kumari^{156b}, A. Kupco¹³¹, T. Kupfer⁴⁹, A. Kupich³⁷, O. Kuprash⁵⁴, H. Kurashige⁸⁵, L. L. Kurchaninov^{156a}, O. Kurdysh⁶⁶, Y. A. Kurochkin³⁷, A. Kurova³⁷, M. Kuze¹⁵⁴, A. K. Kvam¹⁰³, J. Kvita¹²², T. Kwan¹⁰⁴, N. G. Kyriacou¹⁰⁶, L. A. O. Laatu¹⁰², C. Lacasta¹⁶³, F. Lacava^{75a,75b}, H. Lacker¹⁸, D. Lacour¹²⁷, N. N. Lad⁹⁶, E. Ladygin³⁸, B. Laforge¹²⁷, T. Lagouri^{137e}, F. Z. Lahbabi^{35a}, S. Lai⁵⁵, I. K. Lacomiec^{86a}, N. Lalloue⁶⁰, J. E. Lambert¹⁶⁵, S. Lammers⁶⁸, W. Lampl⁷, C. Lampoudis^{152.e}, A. N. Lancaster¹¹⁵, E. Lançon²⁹, U. Landgraf⁵⁴, M. P. J. Landon⁹⁴, V. S. Lang⁵⁴, R. J. Langenberg¹⁰³, O. K. B. Langrekken¹²⁵, A. J. Lankford¹⁶⁰, F. Lanni³⁶, K. Lantzsch²⁴, A. Lanza^{73a}, A. Lapertosa^{57a,57b}, J. F. Laporte¹³⁵, T. Lari^{71a}, F. Lasagni Manghi^{23b}, M. Lassnig³⁶, V. Latonova¹³¹, A. Laudrain¹⁰⁰, A. Laurier¹⁵⁰, S. D. Lawlor¹³⁹, Z. Lawrence¹⁰¹, R. Lazaridou¹⁶⁷, M. Lazzaroni^{71a,71b}, B. Le¹⁰¹, E. M. Le Boulicaut⁵¹, B. Leban⁹³, A. Lebedev⁸¹, M. LeBlanc¹⁰¹, F. Ledroit-Guillon⁶⁰, A. C. A. Lee⁹⁶, S. C. Lee¹⁴⁸, S. Lee^{47a,47b}, T. F. Lee⁹², L. L. Leeuw^{33c}, H. P. Lefebvre⁹⁵, M. Lefebvre¹⁶⁵, C. Leggett^{17a}, G. Lehmann Miotto³⁶, M. Leigh⁵⁶, W. A. Leight¹⁰³, W. Leinonen¹¹³, A. Leisos^{152.r}, M. A. L. Leite^{83c}, C. E. Leitgeb⁴⁸, R. Leitner¹³³, K. J. C. Leney⁴⁴, T. Lenz²⁴, S. Leone^{74a}, C. Leonidopoulos⁵², A. Leopold¹⁴⁴, C. Leroy¹⁰⁸, R. Les¹⁰⁷, C. G. Lester³², M. Levchenko³⁷, J. Levêque⁴, D. Levin¹⁰⁶, L. J. Levinson¹⁶⁹, M. P. Lewicki⁸⁷, D. J. Lewis⁴, A. Li⁵, B. Li^{62b}, C. Li^{62a}, C-Q. Li¹¹⁰, H. Li^{62a}, H. Li^{62b}, H. Li^{14c}, H. Li^{14b}, H. Li^{62b}, J. Li^{62c}, K. Li¹³⁸, L. Li^{62c}, M. Li^{14a,14e}, Q. Y. Li^{62a}, S. Li^{14a,14e}, S. Li^{62c,62d}, T. Li⁵, X. Li¹⁰⁴, Z. Li¹²⁶, Z. Li¹⁰⁴, Z. Li^{14a,14e}, S. Liang^{14a,14e}, Z. Liang^{14a}, M. Liberatore¹³⁵, B. Liberti^{76a}, K. Lie^{64c}, J. Lieber Marin^{83b}, H. Lien⁶⁸, K. Lin¹⁰⁷, R. E. Lindley⁷, J. H. Lindon², E. Lipeles¹²⁸, A. Lipniacka¹⁶, A. Lister¹⁶⁴, J. D. Little⁴, B. Liu^{14a}, B. X. Liu¹⁴², D. Liu^{62c,62d}, J. B. Liu^{62a}, J. K. K. Liu³², K. Liu^{62c,62d}, M. Liu^{62a}, M. Y. Liu^{62a}, P. Liu^{14a}, Q. Liu^{62c,62d,138}, X. Liu^{62a}, X. Liu^{62b}, Y. Liu^{14d,14e}, Y. L. Liu^{62b}, Y. W. Liu^{62a}, J. Llorente Merino¹⁴², S. L. Lloyd⁹⁴, E. M. Lobodzinska⁴⁸, P. Loch⁷, T. Lohse¹⁸, K. Lohwasser¹³⁹, E. Loiacono⁴⁸, M. Lokajicek^{131,*}, J. D. Lomas²⁰, J. D. Long¹⁶², I. Longarini¹⁶⁰, L. Longo^{70a,70b}, R. Longo¹⁶², I. Lopez Paz⁶⁷, A. Lopez Solis⁴⁸, N. Lorenzo Martinez⁴, A. M. Lory¹⁰⁹, G. Löschecke Centeno¹⁴⁶, O. Loseva³⁷, X. Lou^{47a,47b}, X. Lou^{14a,14e}, A. Lounis⁶⁶, J. Love⁶, P. A. Love⁹¹, G. Lu^{14a,14e}, M. Lu⁸⁰, S. Lu¹²⁸, Y. J. Lu⁶⁵, H. J. Lubatti¹³⁸, C. Luci^{75a,75b}, F. L. Lucio Alves^{14c}, A. Lucotte⁶⁰, F. Luehring⁶⁸, I. Luise¹⁴⁵, O. Lukianchuk⁶⁶, O. Lundberg¹⁴⁴, B. Lund-Jensen¹⁴⁴, N. A. Luongo⁶, M. S. Lutz¹⁵¹, A. B. Lux²⁵, D. Lynn²⁹, H. Lyons⁹², R. Lysak¹³¹, E. Lytken⁹⁸, V. Lyubushkin³⁸, T. Lyubushkina³⁸, M. M. Lyukova¹⁴⁵, H. Ma²⁹, K. Ma^{62a}, L. L. Ma^{62b}, W. Ma^{62a}, Y. Ma¹²¹, D. M. Mac Donell¹⁶⁵, G. Maccarrone⁵³, J. C. MacDonald¹⁰⁰, P. C. Machado De Abreu Farias^{83b}, R. Madar⁴⁰, W. F. Mader⁵⁰, T. Madula⁹⁶, J. Maeda⁸⁵, T. Maeno²⁹, H. Maguire¹³⁹, V. Maiboroda¹³⁵, A. Maio^{130a,130b,130d}, K. Maj^{86a}, O. Majersky⁴⁸, S. Majewski¹²³, N. Makovec⁶⁶, V. Maksimovic¹⁵, B. Malaescu¹²⁷, Pa. Malecki⁸⁷, V. P. Maleev³⁷, F. Malek⁶⁰, M. Mali⁹³, D. Malito⁹⁵, U. Mallik⁸⁰, S. Maltezos¹⁰, S. Malyukov³⁸, J. Mamuzic¹³, G. Mancini⁵³, G. Manco^{73a,73b}, J. P. Mandalia⁹⁴, I. Mandić⁹³, L. Manhaes de Andrade Filho^{83a}, I. M. Maniatis¹⁶⁹, J. Manjarres Ramos^{102.aa}, D. C. Mankad¹⁶⁹, A. Mann¹⁰⁹, B. Mansoulie¹³⁵, S. Manzoni³⁶, L. Mao^{62c}, X. Mapekula^{33c}, A. Marantis^{152.r}, G. Marchiori⁵, M. Marcisovsky¹³¹, C. Marcon^{71a}, M. Marinescu²⁰

S. Marium⁴⁸, M. Marjanovic¹²⁰, E. J. Marshall⁹¹, Z. Marshall^{17a}, S. Marti-Garcia¹⁶³, T. A. Martin¹⁶⁷,
 V. J. Martin⁵², B. Martin dit Latour¹⁶, L. Martinelli^{75a,75b}, M. Martinez^{13,s}, P. Martinez Agullo¹⁶³,
 V. I. Martinez Outschoorn¹⁰³, P. Martinez Suarez¹³, S. Martin-Haugh¹³⁴, V. S. Martoiu^{27b}, A. C. Martyniuk⁹⁶,
 A. Marzin³⁶, D. Mascione^{78a,78b}, L. Masetti¹⁰⁰, T. Mashimo¹⁵³, J. Masik¹⁰¹, A. L. Maslennikov³⁷,
 L. Massa^{23b}, P. Massarotti^{72a,72b}, P. Mastrandrea^{74a,74b}, A. Mastroberardino^{43a,43b}, T. Masubuchi¹⁵³,
 T. Mathisen¹⁶¹, J. Matousek¹³³, N. Matsuzawa¹⁵³, J. Maurer^{27b}, B. Maček⁹³, D. A. Maximov³⁷, R. Mazini¹⁴⁸,
 I. Maznas¹⁵², M. Mazza¹⁰⁷, S. M. Mazza¹³⁶, E. Mazzeo^{71a,71b}, C. Mc Ginn²⁹, J. P. Mc Gowan¹⁰⁴,
 S. P. Mc Kee¹⁰⁶, C. C. McCracken¹⁶⁴, E. F. McDonald¹⁰⁵, A. E. McDougall¹¹⁴, J. A. Mcfayden¹⁴⁶,
 R. P. McGovern¹²⁸, G. Mchedlidge^{149b}, R. P. Mckenzie^{33g}, T. C. Mclachlan⁴⁸, D. J. Mclaughlin⁹⁶,
 S. J. McMahan¹³⁴, C. M. Mcpartland⁹², R. A. McPherson^{165,w}, S. Mehlhase¹⁰⁹, A. Mehta⁹², D. Melini¹⁵⁰,
 B. R. Mellado Garcia^{33g}, A. H. Melo⁵⁵, F. Meloni⁴⁸, A. M. Mendes Jacques Da Costa¹⁰¹, H. Y. Meng¹⁵⁵,
 L. Meng⁹¹, S. Menke¹¹⁰, M. Mentink³⁶, E. Meoni^{43a,43b}, G. Mercado¹¹⁵, C. Merlassino^{69a,69c},
 L. Merola^{72a,72b}, C. Meroni^{71a,71b}, G. Merz¹⁰⁶, J. Metcalfe⁶, A. S. Mete⁶, C. Meyer⁶⁸, J-P. Meyer¹³⁵,
 R. P. Middleton¹³⁴, L. Mijović⁵², G. Mikenberg¹⁶⁹, M. Mikesstikova¹³¹, M. Mikuz⁹³, H. Mildner¹⁰⁰,
 A. Milic³⁶, C. D. Milke⁴⁴, D. W. Miller³⁹, L. S. Miller³⁴, A. Milov¹⁶⁹, D. A. Milstead^{47a,47b},
 T. Min^{14c}, A. A. Minaenko³⁷, I. A. Minashvili^{149b}, L. Mince⁵⁹, A. I. Mincer¹¹⁷, B. Mindur^{86a},
 M. Mineev³⁸, Y. Mino⁸⁸, L. M. Mir¹³, M. Miralles Lopez¹⁶³, M. Mironova^{17a}, A. Mishima¹⁵³,
 M. C. Missio¹¹³, A. Mitra¹⁶⁷, V. A. Mitsou¹⁶³, Y. Mitsumori¹¹¹, O. Miu¹⁵⁵, P. S. Miyagawa⁹⁴,
 T. Mkrtychyan^{63a}, M. Mlinarevic⁹⁶, T. Mlinarevic⁹⁶, M. Mlynarikova³⁶, S. Mobius¹⁹, P. Moder⁴⁸,
 P. Mogg¹⁰⁹, M. H. Mohamed Farook¹¹², A. F. Mohammed^{14a,14c}, S. Mohapatra⁴¹, G. Mokgatitswane^{33g},
 L. Moleri¹⁶⁹, B. Mondal¹⁴¹, S. Mondal¹³², K. Mönig⁴⁸, E. Monnier¹⁰², L. Monsonis Romero¹⁶³,
 J. Montejo Berlingen¹³, M. Montella¹¹⁹, F. Montekali^{77a,77b}, F. Monticelli⁹⁰, S. Monzani^{69a,69c},
 N. Morange⁶⁶, A. L. Moreira De Carvalho^{130a}, M. Moreno Llácilcer¹⁶³, C. Moreno Martinez⁵⁶, P. Moretini^{57b},
 S. Morgenstern³⁶, M. Morii⁶¹, M. Morinaga¹⁵³, A. K. Morley³⁶, F. Morodei^{75a,75b}, L. Morvaj³⁶,
 P. Moschovakos³⁶, B. Moser³⁶, M. Mosidze^{149b}, T. Moskalets⁵⁴, P. Moskvitina¹¹³, J. Moss^{31,l},
 E. J. W. Moyse¹⁰³, O. Mtintsilana^{33g}, S. Muanza¹⁰², J. Mueller¹²⁹, D. Muenstermann⁹¹, R. Müller¹⁹,
 G. A. Mullier¹⁶¹, A. J. Mullin³², J. J. Mullin¹²⁸, D. P. Mungo¹⁵⁵, D. Munoz Perez¹⁶³, F. J. Munoz Sanchez¹⁰¹,
 M. Murin¹⁰¹, W. J. Murray^{134,167}, A. Murrone^{71a,71b}, M. Muškinja^{17a}, C. Mwewa²⁹, A. G. Myagkov^{37,a},
 A. J. Myers⁸, G. Myers⁶⁸, M. Myska¹³², B. P. Nachman^{17a}, O. Nackenhorst⁴⁹, A. Nag⁵⁰, K. Nagai¹²⁶,
 K. Nagano⁸⁴, J. L. Nagle^{29,ai}, E. Nagy¹⁰², A. M. Nairz³⁶, Y. Nakahama⁸⁴, K. Nakamura⁸⁴, K. Nakkalil⁵,
 H. Nanjo¹²⁴, R. Narayan⁴⁴, E. A. Narayanan¹¹², I. Naryshkin³⁷, M. Naseri³⁴, S. Nasri¹⁵⁹, C. Nass²⁴,
 G. Navarro^{22a}, J. Navarro-Gonzalez¹⁶³, R. Nayak¹⁵¹, A. Nayaz¹⁸, P. Y. Nechaeva³⁷, F. Nechansky⁴⁸,
 L. Nedic¹²⁶, T. J. Neep²⁰, A. Negri^{73a,73b}, M. Negrini^{23b}, C. Nellist¹¹⁴, C. Nelson¹⁰⁴, K. Nelson¹⁰⁶,
 S. Nemecek¹³¹, M. Nessi^{36,h}, M. S. Neubauer¹⁶², F. Neuhaus¹⁰⁰, J. Neundorff⁴⁸, R. Newhouse¹⁶⁴,
 P. R. Newman²⁰, C. W. Ng¹²⁹, Y. W. Y. Ng⁴⁸, B. Ngair^{35e}, H. D. N. Nguyen¹⁰⁸, R. B. Nickerson¹²⁶,
 R. Nicolaidou¹³⁵, J. Nielsen¹³⁶, M. Niemeyer⁵⁵, J. Niermann^{36,55}, N. Nikiforou³⁶, V. Nikolaenko^{37,a},
 I. Nikolic-Audit¹²⁷, K. Nikolopoulos²⁰, P. Nilsson²⁹, I. Ninca⁴⁸, H. R. Nindhito⁵⁶, G. Ninio¹⁵¹,
 A. Nisati^{75a}, N. Nishu², R. Nisius¹¹⁰, J-E. Nitschke⁵⁰, E. K. Nkadimeng^{33g}, T. Nobe¹⁵³, D. L. Noel³²,
 T. Nommensen¹⁴⁷, M. B. Norfolk¹³⁹, R. R. B. Norisam⁹⁶, B. J. Norman³⁴, M. Noury^{35a}, J. Novak⁹³,
 T. Novak⁴⁸, L. Novotny¹³², R. Novotny¹¹², L. Nozka¹²², K. Ntekas¹⁶⁰, N. M. J. Nunes De Moura Junior^{83b},
 E. Nurse⁹⁶, J. Ocariz¹²⁷, A. Ochi⁸⁵, I. Ochoa^{130a}, S. Oerdek^{48,t}, J. T. Offermann³⁹, A. Ogrodnik¹³³,
 A. Oh¹⁰¹, C. C. Ohm¹⁴⁴, H. Oide⁸⁴, R. Oishi¹⁵³, M. L. Ojeda⁴⁸, M. W. O’Keefe⁹², Y. Okumura¹⁵³,
 L. F. Oleiro Seabra^{130a}, S. A. Olivares Pino^{137d}, D. Oliveira Damazio²⁹, D. Oliveira Goncalves^{83a},
 J. L. Oliver¹⁶⁰, Ö. Ö. Öncel⁵⁴, A. P. O’Neill¹⁹, A. Onofre^{130a,130e}, P. U. E. Onyisi¹¹, M. J. Oreglia³⁹,
 G. E. Orellana⁹⁰, D. Orestano^{77a,77b}, N. Orlando¹³, R. S. Orr¹⁵⁵, V. O’Shea⁵⁹, L. M. Osojnak¹²⁸,
 R. Ospanov^{62a}, G. Otero y Garzon³⁰, H. Otono⁸⁹, P. S. Ott^{63a}, G. J. Ottino^{17a}, M. Ouchrif^{35d}, J. Ouellette²⁹,
 F. Ould-Saada¹²⁵, M. Owen⁵⁹, R. E. Owen¹³⁴, K. Y. Oyulmaz^{21a}, V. E. Ozcan^{21a}, F. Ozturk⁸⁷, N. Ozturk⁸,
 S. Ozturk⁸², H. A. Pacey¹²⁶, A. Pacheco Pages¹³, C. Padilla Aranda¹³, G. Padovano^{75a,75b}, S. Pagan Griso^{17a},
 G. Palacino⁶⁸, A. Palazzo^{70a,70b}, S. Palestini³⁶, J. Pan¹⁷², T. Pan^{64a}, D. K. Panchal¹¹, C. E. Pandini¹¹⁴,
 J. G. Panduro Vazquez⁹⁵, H. D. Pandya¹, H. Pang^{14b}, P. Pani⁴⁸, G. Panizzo^{69a,69c}, L. Paolozzi⁵⁶,
 C. Papadatos¹⁰⁸, S. Parajuli⁴⁴, A. Paramonov⁶, C. Paraskevopoulos¹⁰, D. Paredes Hernandez^{64b}, K. R. Park⁴¹,
 T. H. Park¹⁵⁵, M. A. Parker³², F. Parodi^{57a,57b}, E. W. Parrish¹¹⁵, V. A. Parrish⁵², J. A. Parsons⁴¹,
 U. Parzefall⁵⁴, B. Pascual Dias¹⁰⁸, L. Pascual Dominguez¹⁵¹, E. Pasqualucci^{75a}, S. Passaggio^{57b},

C. Schmitt¹⁰⁰, N. Schmitt¹⁰⁰, S. Schmitt⁴⁸, L. Schoeffel¹³⁵, A. Schoening^{63b}, P. G. Scholer⁵⁴, E. Schopf¹²⁶, M. Schott¹⁰⁰, J. Schovancova³⁶, S. Schramm⁵⁶, F. Schroeder¹⁷¹, T. Schroer⁵⁶, H-C. Schultz-Coulon^{63a}, M. Schumacher⁵⁴, B. A. Schumm¹³⁶, Ph. Schune¹³⁵, A. J. Schuy¹³⁸, H. R. Schwartz¹³⁶, A. Schwartzman¹⁴³, T. A. Schwarz¹⁰⁶, Ph. Schwemling¹³⁵, R. Schwienhorst¹⁰⁷, A. Sciandra¹³⁶, G. Sciolla²⁶, F. Scuri^{74a}, C. D. Sebastiani⁹², K. Sedlaczek¹¹⁵, P. Seema¹⁸, S. C. Seidel¹¹², A. Seiden¹³⁶, B. D. Seidlitz⁴¹, C. Seitz⁴⁸, J. M. Seixas^{83b}, G. Sekhniaidze^{72a}, S. J. Sekula⁴⁴, L. Selem⁶⁰, N. Semprini-Cesari^{23a,23b}, D. Sengupta⁵⁶, V. Senthilkumar¹⁶³, L. Serin⁶⁶, L. Serkin^{69a,69b}, M. Sessa^{76a,76b}, H. Severini¹²⁰, F. Sforza^{57a,57b}, A. Sfyrta⁵⁶, E. Shabalina⁵⁵, R. Shaheen¹⁴⁴, J. D. Shahinian¹²⁸, D. Shaked Renous¹⁶⁹, L. Y. Shan^{14a}, M. Shapiro^{17a}, A. Sharma³⁶, A. S. Sharma¹⁶⁴, P. Sharma⁸⁰, S. Sharma⁴⁸, P. B. Shatalov³⁷, K. Shaw¹⁴⁶, S. M. Shaw¹⁰¹, A. Shcherbakova³⁷, Q. Shen^{5,62c}, D. J. Sheppard¹⁴², P. Sherwood⁹⁶, L. Shi⁹⁶, X. Shi^{14a}, C. O. Shimmin¹⁷², J. D. Shinner⁹⁵, I. P. J. Shipsey¹²⁶, S. Shirabe^{56,h}, M. Shiyakova^{38,u}, J. Shlomi¹⁶⁹, M. J. Shochet³⁹, J. Shojaii¹⁰⁵, D. R. Shope¹²⁵, B. Shrestha¹²⁰, S. Shrestha^{119,aj}, E. M. Shrif^{33g}, M. J. Shroff¹⁶⁵, P. Sicho¹³¹, A. M. Sickles¹⁶², E. Sideras Haddad^{33g}, A. Sidoti^{23b}, F. Siegert⁵⁰, Dj. Sijacki¹⁵, F. Sili⁹⁰, J. M. Silva²⁰, M. V. Silva Oliveira²⁹, S. B. Silverstein^{47a}, S. Simion⁶⁶, R. Simoniello³⁶, E. L. Simpson⁵⁹, H. Simpson¹⁴⁶, L. R. Simpson¹⁰⁶, N. D. Simpson⁹⁸, S. Simsek⁸², S. Sindhu⁵⁵, P. Sinervo¹⁵⁵, S. Singh¹⁵⁵, S. Sinha⁴⁸, S. Sinha¹⁰¹, M. Sioli^{23a,23b}, I. Siral³⁶, E. Sitnikova⁴⁸, S. Yu. Sivoklokov^{37,*}, J. Sjölin^{47a,47b}, A. Skaf⁵⁵, E. Skorda²⁰, P. Skubic¹²⁰, M. Slawinska⁸⁷, V. Smakhtin¹⁶⁹, B. H. Smart¹³⁴, J. Smiesko³⁶, S. Yu. Smirnov³⁷, Y. Smirnov³⁷, L. N. Smirnova^{37,a}, O. Smirnova⁹⁸, A. C. Smith⁴¹, E. A. Smith³⁹, H. A. Smith¹²⁶, J. L. Smith⁹², R. Smith¹⁴³, M. Smizanska⁹¹, K. Smolek¹³², A. A. Snesarev³⁷, S. R. Snider¹⁵⁵, H. L. Snoek¹¹⁴, S. Snyder²⁹, R. Sobie^{165,w}, A. Soffer¹⁵¹, C. A. Solans Sanchez³⁶, E. Yu. Soldatov³⁷, U. Soldevila¹⁶³, A. A. Solodkov³⁷, S. Solomon²⁶, A. Soloshenko³⁸, K. Solovieva⁵⁴, O. V. Solovyanov⁴⁰, V. Solovyev³⁷, P. Sommer³⁶, A. Sonay¹³, W. Y. Song^{156b}, J. M. Sonneveld¹¹⁴, A. Sopczak¹³², A. L. Sopio⁹⁶, F. Sopkova^{28b}, I. R. Sotarriva Alvarez¹⁵⁴, V. Sothilingam^{63a}, O. J. Soto Sandoval^{137b,137c}, S. Sottocornola⁶⁸, R. Soualah^{116b}, Z. Soumami^{35e}, D. South⁴⁸, N. Soybelman¹⁶⁹, S. Spagnolo^{70a,70b}, M. Spalla¹¹⁰, D. Sperlich⁵⁴, G. Spigo³⁶, S. Spinali⁹¹, D. P. Spiteri⁵⁹, M. Spusta¹³³, E. J. Staats³⁴, A. Stabile^{71a,71b}, R. Stamen^{63a}, A. Stampekis²⁰, M. Standke²⁴, E. Stanecka⁸⁷, M. V. Stange⁵⁰, B. Stanislaus^{17a}, M. M. Stanitzki⁴⁸, B. Stapf⁴⁸, E. A. Starchenko³⁷, G. H. Stark¹³⁶, J. Stark^{102,aa}, D. M. Starke^{156b}, P. Staroba¹³¹, P. Starovoitov^{63a}, S. Stärz¹⁰⁴, R. Staszewski⁸⁷, G. Stavropoulos⁴⁶, J. Steentoft¹⁶¹, P. Steinberg²⁹, B. Stelzer^{142,156a}, H. J. Stelzer¹²⁹, O. Stelzer-Chilton^{156a}, H. Stenzel⁵⁸, T. J. Stevenson¹⁴⁶, G. A. Stewart³⁶, J. R. Stewart¹²¹, M. C. Stockton³⁶, G. Stoicea^{27b}, M. Stolarski^{130a}, S. Stonjek¹¹⁰, A. Straessner⁵⁰, J. Strandberg¹⁴⁴, S. Strandberg^{47a,47b}, M. Stratmann¹⁷¹, M. Strauss¹²⁰, T. Streblner¹⁰², P. Strizenc^{28b}, R. Ströhmer¹⁶⁶, D. M. Strom¹²³, R. Stroynowski⁴⁴, A. Strubig^{47a,47b}, S. A. Stucci²⁹, B. Stugu¹⁶, J. Stupak¹²⁰, N. A. Styles⁴⁸, D. Su¹⁴³, S. Su^{62a}, W. Su^{62d}, X. Su^{62a,66}, K. Sugizaki¹⁵³, V. V. Sulin³⁷, M. J. Sullivan⁹², D. M. S. Sultan^{78a,78b}, L. Sultanalieva³⁷, S. Sultansoy^{3b}, T. Sumida⁸⁸, S. Sun¹⁰⁶, S. Sun¹⁷⁰, O. Sunneborn Gudnadottir¹⁶¹, N. Sur¹⁰², M. R. Sutton¹⁴⁶, H. Suzuki¹⁵⁷, M. Svatos¹³¹, M. Swiatlowski^{156a}, T. Swirski¹⁶⁶, I. Sykora^{28a}, M. Sykora¹³³, T. Sykora¹³³, D. Ta¹⁰⁰, K. Tackmann^{48,t}, A. Taffard¹⁶⁰, R. Tafirout^{156a}, J. S. Tafoya Vargas⁶⁶, E. P. Takeva⁵², Y. Takubo⁸⁴, M. Talby¹⁰², A. A. Talyshv³⁷, K. C. Tam^{64b}, N. M. Tamir¹⁵¹, A. Tanaka¹⁵³, J. Tanaka¹⁵³, R. Tanaka⁶⁶, M. Tanasini^{57a,57b}, Z. Tao¹⁶⁴, S. Tapia Araya^{137f}, S. Tapprogge¹⁰⁰, A. Tarek Abouelfadl Mohamed¹⁰⁷, S. Tarem¹⁵⁰, K. Tariq^{14a}, G. Tarna^{27b,102}, G. F. Tartarelli^{71a}, P. Tas¹³³, M. Tasevsky¹³¹, E. Tassi^{43a,43b}, A. C. Tate¹⁶², G. Tateno¹⁵³, Y. Tayalati^{35e,v}, G. N. Taylor¹⁰⁵, W. Taylor^{156b}, A. S. Tee¹⁷⁰, R. Teixeira De Lima¹⁴³, P. Teixeira-Dias⁹⁵, J. J. Teoh¹⁵⁵, K. Terashi¹⁵³, J. Terron⁹⁹, S. Terzo¹³, M. Testa⁵³, R. J. Teuscher^{155,w}, A. Thaler⁷⁹, O. Theiner⁵⁶, N. Themistokleous⁵², T. Theveneaux-Pelzer¹⁰², O. Thielmann¹⁷¹, D. W. Thomas⁹⁵, J. P. Thomas²⁰, E. A. Thompson^{17a}, P. D. Thompson²⁰, E. Thomson¹²⁸, Y. Tian⁵⁵, V. Tikhomirov^{37,a}, Yu. A. Tikhonov³⁷, S. Timoshenko³⁷, D. Timoshyn¹³³, E. X. L. Ting¹, P. Tipton¹⁷², S. H. Tlou^{33g}, A. Tnourji⁴⁰, K. Todome¹⁵⁴, S. Todorova-Nova¹³³, S. Todt⁵⁰, M. Togawa⁸⁴, J. Tojo⁸⁹, S. Tokár^{28a}, K. Tokushuku⁸⁴, O. Toldaiev⁶⁸, R. Tombs³², M. Tomoto^{84,111}, L. Tompkins^{143,n}, K. W. Topolnicki^{86b}, E. Torrence¹²³, H. Torres^{102,aa}, E. Torró Pastor¹⁶³, M. Toscani³⁰, C. Toscirri³⁹, M. Tost¹¹, D. R. Tovey¹³⁹, A. Traet¹⁶, I. S. Trandafir^{27b}, T. Trefzger¹⁶⁶, A. Tricoli²⁹, I. M. Trigger^{156a}, S. Trincz-Duvold¹²⁷, D. A. Trischuk²⁶, B. Trocme⁶⁰, C. Troncon^{71a}, L. Truong^{33c}, M. Trzebinski⁸⁷, A. Trzupek⁸⁷, F. Tsai¹⁴⁵, M. Tsai¹⁰⁶, A. Tsiamis^{152,e}, P. V. Tsiarehka³⁷, S. Tsigaridas^{156a}, A. Tsirigotis^{152,r}, V. Tsiskaridze¹⁵⁵, E. G. Tskhadadze^{149a}, M. Tsopoulou^{152,e}, Y. Tsujikawa⁸⁸, I. I. Tsukerman³⁷, V. Tsulaia^{17a}, S. Tsuno⁸⁴, K. Tsuru¹¹⁸, D. Tsybychev¹⁴⁵, Y. Tu^{64b}, A. Tudorache^{27b}, V. Tudorache^{27b}

A. N. Tuna⁶¹, S. Turchikhin^{57a,57b}, I. Turk Cakir^{3a}, R. Turra^{71a}, T. Turtuvshin^{38,x}, P. M. Tuts⁴¹, S. Tzamarias^{152,e}, P. Tzanis¹⁰, E. Tzovara¹⁰⁰, F. Ukegawa¹⁵⁷, P. A. Ulloa Poblete^{137b,137c}, E. N. Umaka²⁹, G. Unal³⁶, M. Unal¹¹, A. Undrus²⁹, G. Unel¹⁶⁰, J. Urban^{28b}, P. Urquijo¹⁰⁵, P. Urrejola^{137a}, G. Usai⁸, R. Ushioda¹⁵⁴, M. Usman¹⁰⁸, Z. Uysal^{21b}, V. Vacek¹³², B. Vachon¹⁰⁴, K. O. H. Vadla¹²⁵, T. Vafeiadis³⁶, A. Vaitkus⁹⁶, C. Valderanis¹⁰⁹, E. Valdes Santurio^{47a,47b}, M. Valente^{156a}, S. Valentinetti^{23a,23b}, A. Valero¹⁶³, E. Valiente Moreno¹⁶³, A. Vallier^{102,aa}, J. A. Valls Ferrer¹⁶³, D. R. Van Arneeman¹¹⁴, T. R. Van Daalen¹³⁸, A. Van Der Graaf⁴⁹, P. Van Gemmeren⁶, M. Van Rijnbach^{36,125}, S. Van Stroud⁹⁶, I. Van Vulpen¹¹⁴, M. Vanadia^{76a,76b}, W. Vandelli³⁶, M. Vandenbroucke¹³⁵, E. R. Vandewall¹²¹, D. Vannicola¹⁵¹, L. Vannoli^{57a,57b}, R. Vari^{75a}, E. W. Varnes⁷, C.
Varni^{17b}, T. Varol¹⁴⁸, D. Varouchas⁶⁶, L. Varriale¹⁶³, K. E. Varvell¹⁴⁷, M. E. Vasile^{27b}, L. Vaslin⁸⁴, G. A. Vasquez¹⁶⁵, A. Vasyukov³⁸, F. Vazeille⁴⁰, T. Vazquez Schroeder³⁶, J. Veatch³¹, V. Vecchio¹⁰¹, M. J. Veen¹⁰³, I. Veliscek¹²⁶, L. M. Veloce¹⁵⁵, F. Veloso^{130a,130c}, S. Veneziano^{75a}, A. Ventura^{70a,70b}, S. Ventura Gonzalez¹³⁵, A. Verbytskyi¹¹⁰, M. Verducci^{74a,74b}, C. Vergis²⁴, M. Verissimo De Araujo^{83b}, W. Verkerke¹¹⁴, J. C. Vermeulen¹¹⁴, C. Vernieri¹⁴³, M. Vessella¹⁰³, M. C. Vetterli^{142,af}, A. Vgenopoulos^{152,e}, N. Viaux Maira^{137f}, T. Vickey¹³⁹, O. E. Vickey Boeriu¹³⁹, G. H. A. Viehhauser¹²⁶, L. Vigani^{63b}, M. Villa^{23a,23b}, M. Villaplana Perez¹⁶³, E. M. Villhauer⁵², E. Vilucchi⁵³, M. G. Vinciter³⁴, G. S. Virdee²⁰, A. Vishwakarma⁵², A. Visibile¹¹⁴, C. Vittori³⁶, I. Vivarelli¹⁴⁶, E. Voevodina¹¹⁰, F. Vogel¹⁰⁹, J. C. Voigt⁵⁰, P. Vokac¹³², Yu. Volkotrub^{86a}, J. Von Ahnen⁴⁸, E. Von
Toerne²⁴, B. Vormwald³⁶, V. Vorobel¹³³, K. Vorobev³⁷, M. Vos¹⁶³, K. Voss¹⁴¹, J. H. Vosseveld⁹², M. Vozak¹¹⁴, L. Vozdecky⁹⁴, N. Vranjes¹⁵, M. Vranjes Milosavljevic¹⁵, M. Vreeswijk¹¹⁴, R. Vuillermet³⁶, O. Vujanovic¹⁰⁰, I. Vukotic³⁹, S. Wada¹⁵⁷, C. Wagner¹⁰³, J. M. Wagner^{17a}, W. Wagner¹⁷¹, S. Wahdan¹⁷¹, H. Wahlberg⁹⁰, M. Wakida¹¹¹, J. Walder¹³⁴, R. Walker¹⁰⁹, W. Walkowiak¹⁴¹, A. Wall¹²⁸, T. Wamorkar⁶, A. Z. Wang¹³⁶, C. Wang¹⁰⁰, C. Wang^{62c}, H. Wang^{17a}, J. Wang^{64a}, R.-J. Wang¹⁰⁰, R. Wang⁶¹, R. Wang⁶, S. M. Wang¹⁴⁸, S. Wang^{62b}, T. Wang^{62a}, W. T. Wang⁸⁰, W. Wang^{14a}, X. Wang^{14c}, X. Wang¹⁶², X. Wang^{62e}, Y. Wang^{62d}, Y. Wang^{14c}, Z. Wang¹⁰⁶, Z. Wang^{51,62c,62d}, Z. Wang¹⁰⁶, A. Warburton¹⁰⁴, R. J. Ward²⁰, N. Warrack⁵⁹, A. T. Watson²⁰, H.
Watson⁵⁹, M. F. Watson²⁰, E. Watton^{59,134}, G. Watts¹³⁸, B. M. Waugh⁹⁶, C. Weber²⁹, H. A. Weber¹⁸, M. S. Weber¹⁹, S. M. Weber^{63a}, C. Wei^{62a}, Y. Wei¹²⁶, A. R. Weidberg¹²⁶, E. J. Weik¹¹⁷, J. Weingarten⁴⁹, M. Weirich¹⁰⁰, C. Weiser⁵⁴, C. J. Wells⁴⁸, T. Wenaus²⁹, B. Wendland⁴⁹, T. Wengler³⁶, N. S. Wenke¹¹⁰, N. Wermes²⁴, M. Wessels^{63a}, A. M. Wharton⁹¹, A. S. White⁶¹, A. White⁸, M. J. White¹, D. Whiteson¹⁶⁰, L. Wickremasinghe¹²⁴, W. Wiedenmann¹⁷⁰, C. Wiel⁵⁰, M. Wielers¹³⁴, C. Wiglesworth⁴², D. J. Wilbern¹²⁰, H. G. Wilkens³⁶, D. M. Williams⁴¹, H. H. Williams¹²⁸, S. Williams³², S. Willocq¹⁰³, B. J. Wilson¹⁰¹, P. J. Windischhofer³⁹, F. I. Winkel³⁰, F. Winklmeier¹²³, B. T. Winter⁵⁴, J. K. Winter¹⁰¹, M. Wittgen¹⁴³, M. Wobisch⁹⁷, Z. Wolffs¹¹⁴, J. Wollrath¹⁶⁰, M. W. Wolter⁸⁷, H. Wolters^{130a,130c}, A. F. Wongel⁴⁸, E. L.
Woodward⁴¹, S. D. Worm⁴⁸, B. K. Wosiek⁸⁷, K. W. Woźniak⁸⁷, S. Wozniowski⁵⁵, K. Wraight⁵⁹, C. Wu²⁰, J. Wu^{14a,14c}, M. Wu^{64a}, M. Wu¹¹³, S. L. Wu¹⁷⁰, X. Wu⁵⁶, Y. Wu^{62a}, Z. Wu¹³⁵, J. Wuerzinger^{110,ad}, T. R. Wyatt¹⁰¹, B. M. Wynne⁵², S. Xella⁴², L. Xia^{14c}, M. Xia^{14b}, J. Xiang^{64c}, M. Xie^{62a}, X. Xie^{62a}, S. Xin^{14a,14e}, A. Xiong¹²³, J. Xiong^{17a}, D. Xu^{14a}, H. Xu^{62a}, L. Xu^{62a}, R. Xu¹²⁸, T. Xu¹⁰⁶, Y. Xu^{14b}, Z. Xu⁵², Z. Xu^{14c}, B. Yabsley¹⁴⁷, S. Yacoub^{33a}, Y. Yamaguchi¹⁵⁴, E. Yamashita¹⁵³, H. Yamauchi¹⁵⁷, T. Yamazaki^{17a}, Y. Yamazaki⁸⁵, J. Yan^{62c}, S. Yan¹²⁶, Z. Yan²⁵, H. J. Yang^{62c,62d}, H. T. Yang^{62a}, S. Yang^{62a}, T. Yang^{64c}, X. Yang³⁶, X. Yang^{14a}, Y. Yang⁴⁴, Y. Yang^{62a}, Z.
Yang^{62a}, W.-M. Yao^{17a}, Y. C. Yap⁴⁸, H. Ye^{14c}, H. Ye⁵⁵, J. Ye^{14a}, S. Ye²⁹, X. Ye^{62a}, Y. Yeh⁹⁶, I. Yeletsikh³⁸, B. K. Yeo^{17b}, M. R. Yexley⁹⁶, P. Yin⁴¹, K. Yorita¹⁶⁸, S. Younas^{27b}, C. J. S. Young³⁶, C. Young¹⁴³, C. Yu^{14a,14c,ah}, Y. Yu^{62a}, M. Yuan¹⁰⁶, R. Yuan^{62b}, L. Yue⁹⁶, M. Zaazoua^{62a}, B. Zabinski⁸⁷, E. Zaid⁵², Z. K. Zak⁸⁷, T. Zakareishvili^{149b}, N. Zakharchuk³⁴, S. Zambito⁵⁶, J. A. Zamora Saa^{137b,137d}, J. Zang¹⁵³, D. Zanzi⁵⁴, O. Zaplatilek¹³², C. Zeitnitz¹⁷¹, H. Zeng^{14a}, J. C. Zeng¹⁶², D. T. Zenger Jr²⁶

- ¹ Department of Physics, University of Adelaide, Adelaide, Australia
- ² Department of Physics, University of Alberta, Edmonton, AB, Canada
- ³ ^(a)Department of Physics, Ankara University, Ankara, Türkiye; ^(b)Division of Physics, TOBB University of Economics and Technology, Ankara, Türkiye
- ⁴ LAPP, Université Savoie Mont Blanc, CNRS/IN2P3, Annecy, France
- ⁵ APC, Université Paris Cité, CNRS/IN2P3, Paris, France
- ⁶ High Energy Physics Division, Argonne National Laboratory, Argonne, IL, USA
- ⁷ Department of Physics, University of Arizona, Tucson, AZ, USA
- ⁸ Department of Physics, University of Texas at Arlington, Arlington, TX, USA
- ⁹ Physics Department, National and Kapodistrian University of Athens, Athens, Greece
- ¹⁰ Physics Department, National Technical University of Athens, Zografou, Greece
- ¹¹ Department of Physics, University of Texas at Austin, Austin, TX, USA
- ¹² Institute of Physics, Azerbaijan Academy of Sciences, Baku, Azerbaijan
- ¹³ Institut de Física d'Altes Energies (IFAE), Barcelona Institute of Science and Technology, Barcelona, Spain
- ¹⁴ ^(a)Institute of High Energy Physics, Chinese Academy of Sciences, Beijing, China; ^(b)Physics Department, Tsinghua University, Beijing, China; ^(c)Department of Physics, Nanjing University, Nanjing, China; ^(d)School of Science, Shenzhen Campus of Sun Yat-sen University, Shenzhen, China; ^(e)University of Chinese Academy of Science (UCAS), Beijing, China
- ¹⁵ Institute of Physics, University of Belgrade, Belgrade, Serbia
- ¹⁶ Department for Physics and Technology, University of Bergen, Bergen, Norway
- ¹⁷ ^(a)Physics Division, Lawrence Berkeley National Laboratory, Berkeley, CA, USA; ^(b)University of California, Berkeley, CA, USA
- ¹⁸ Institut für Physik, Humboldt Universität zu Berlin, Berlin, Germany
- ¹⁹ Albert Einstein Center for Fundamental Physics and Laboratory for High Energy Physics, University of Bern, Bern, Switzerland
- ²⁰ School of Physics and Astronomy, University of Birmingham, Birmingham, UK
- ²¹ ^(a)Department of Physics, Bogazici University, Istanbul, Türkiye; ^(b)Department of Physics Engineering, Gaziantep University, Gaziantep, Türkiye; ^(c)Department of Physics, Istanbul University, Istanbul, Türkiye
- ²² ^(a)Facultad de Ciencias y Centro de Investigaciones, Universidad Antonio Nariño, Bogotá, Colombia; ^(b)Departamento de Física, Universidad Nacional de Colombia, Bogotá, Colombia
- ²³ ^(a)Dipartimento di Fisica e Astronomia A. Righi, Università di Bologna, Bologna, Italy; ^(b)INFN Sezione di Bologna, Bologna, Italy
- ²⁴ Physikalisches Institut, Universität Bonn, Bonn, Germany
- ²⁵ Department of Physics, Boston University, Boston, MA, USA
- ²⁶ Department of Physics, Brandeis University, Waltham, MA, USA
- ²⁷ ^(a)Transilvania University of Brasov, Brasov, Romania; ^(b)Horia Hulubei National Institute of Physics and Nuclear Engineering, Bucharest, Romania; ^(c)Department of Physics, Alexandru Ioan Cuza University of Iasi, Iasi, Romania; ^(d)Physics Department, National Institute for Research and Development of Isotopic and Molecular Technologies, Cluj-Napoca, Romania; ^(e)National University of Science and Technology Politehnica, Bucharest, Romania; ^(f)West University in Timisoara, Timisoara, Romania; ^(g)Faculty of Physics, University of Bucharest, Bucharest, Romania
- ²⁸ ^(a)Faculty of Mathematics, Physics and Informatics, Comenius University, Bratislava, Slovakia; ^(b)Department of Subnuclear Physics, Institute of Experimental Physics of the Slovak Academy of Sciences, Kosice, Slovak Republic
- ²⁹ Physics Department, Brookhaven National Laboratory, Upton, NY, USA
- ³⁰ Departamento de Física, y CONICET, Instituto de Física de Buenos Aires (IFIBA), Universidad de Buenos Aires, Facultad de Ciencias Exactas y Naturales, Buenos Aires, Argentina
- ³¹ California State University, Los Angeles, CA, USA
- ³² Cavendish Laboratory, University of Cambridge, Cambridge, UK
- ³³ ^(a)Department of Physics, University of Cape Town, Cape Town, South Africa; ^(b)iThemba Labs, Western Cape, South Africa; ^(c)Department of Mechanical Engineering Science, University of Johannesburg, Johannesburg, South Africa; ^(d)National Institute of Physics, University of the Philippines, Diliman, Philippines; ^(e)Department of Physics, University of South Africa, Pretoria, South Africa; ^(f)University of Zululand, KwaDlangezwa, South Africa; ^(g)School of Physics, University of the Witwatersrand, Johannesburg, South Africa

- ³⁴ Department of Physics, Carleton University, Ottawa, ON, Canada
- ³⁵ ^(a)Faculté des Sciences Ain Chock, Réseau Universitaire de Physique des Hautes Energies-Université Hassan II, Casablanca, Morocco; ^(b)Faculté des Sciences, Université Ibn-Tofail, Kénitra, Morocco; ^(c)Faculté des Sciences Semlalia, Université Cadi Ayyad, LPHEA-Marrakech, Morocco; ^(d)LPMR, Faculté des Sciences, Université Mohamed Premier, Oujda, Morocco; ^(e)Faculté des sciences, Université Mohammed V, Rabat, Morocco; ^(f)Institute of Applied Physics, Mohammed VI Polytechnic University, Ben Guerir, Morocco
- ³⁶ CERN, Geneva, Switzerland
- ³⁷ Affiliated with an Institute Covered by a Cooperation Agreement with CERN, Geneva, Switzerland
- ³⁸ Affiliated with an International Laboratory Covered by a Cooperation Agreement with CERN, Geneva, Switzerland
- ³⁹ Enrico Fermi Institute, University of Chicago, Chicago, IL, USA
- ⁴⁰ LPC, Université Clermont Auvergne, CNRS/IN2P3, Clermont-Ferrand, France
- ⁴¹ Nevis Laboratory, Columbia University, Irvington, NY, USA
- ⁴² Niels Bohr Institute, University of Copenhagen, Copenhagen, Denmark
- ⁴³ ^(a)Dipartimento di Fisica, Università della Calabria, Rende, Italy; ^(b)INFN Gruppo Collegato di Cosenza, Laboratori Nazionali di Frascati, Frascati, Italy
- ⁴⁴ Physics Department, Southern Methodist University, Dallas, TX, USA
- ⁴⁵ Physics Department, University of Texas at Dallas, Richardson, TX, USA
- ⁴⁶ National Centre for Scientific Research “Demokritos”, Agia Paraskevi, Greece
- ⁴⁷ ^(a)Department of Physics, Stockholm University, Stockholm, Sweden; ^(b)Oskar Klein Centre, Stockholm, Sweden
- ⁴⁸ Deutsches Elektronen-Synchrotron DESY, Hamburg and Zeuthen, Germany
- ⁴⁹ Fakultät Physik, Technische Universität Dortmund, Dortmund, Germany
- ⁵⁰ Institut für Kern- und Teilchenphysik, Technische Universität Dresden, Dresden, Germany
- ⁵¹ Department of Physics, Duke University, Durham, NC, USA
- ⁵² SUPA-School of Physics and Astronomy, University of Edinburgh, Edinburgh, UK
- ⁵³ INFN e Laboratori Nazionali di Frascati, Frascati, Italy
- ⁵⁴ Physikalisches Institut, Albert-Ludwigs-Universität Freiburg, Freiburg, Germany
- ⁵⁵ II. Physikalisches Institut, Georg-August-Universität Göttingen, Göttingen, Germany
- ⁵⁶ Département de Physique Nucléaire et Corpusculaire, Université de Genève, Geneva, Switzerland
- ⁵⁷ ^(a)Dipartimento di Fisica, Università di Genova, Genoa, Italy; ^(b)INFN Sezione di Genova, Genoa, Italy
- ⁵⁸ II. Physikalisches Institut, Justus-Liebig-Universität Giessen, Giessen, Germany
- ⁵⁹ SUPA-School of Physics and Astronomy, University of Glasgow, Glasgow, UK
- ⁶⁰ LPSC, Université Grenoble Alpes, CNRS/IN2P3, Grenoble INP, Grenoble, France
- ⁶¹ Laboratory for Particle Physics and Cosmology, Harvard University, Cambridge, MA, USA
- ⁶² ^(a)Department of Modern Physics and State Key Laboratory of Particle Detection and Electronics, University of Science and Technology of China, Hefei, China; ^(b)Institute of Frontier and Interdisciplinary Science and Key Laboratory of Particle Physics and Particle Irradiation (MOE), Shandong University, Qingdao, China; ^(c)School of Physics and Astronomy, Shanghai Jiao Tong University, Key Laboratory for Particle Astrophysics and Cosmology (MOE), SKLPPC, Shanghai, China; ^(d)Tsung-Dao Lee Institute, Shanghai, China; ^(e)School of Physics and Microelectronics, Zhengzhou University, Zhengzhou, China
- ⁶³ ^(a)Kirchhoff-Institut für Physik, Ruprecht-Karls-Universität Heidelberg, Heidelberg, Germany; ^(b)Physikalisches Institut, Ruprecht-Karls-Universität Heidelberg, Heidelberg, Germany
- ⁶⁴ ^(a)Department of Physics, Chinese University of Hong Kong, Shatin, N.T., Hong Kong, China; ^(b)Department of Physics, University of Hong Kong, Hong Kong, China; ^(c)Department of Physics and Institute for Advanced Study, Hong Kong University of Science and Technology, Clear Water Bay, Kowloon, Hong Kong, China
- ⁶⁵ Department of Physics, National Tsing Hua University, Hsinchu, Taiwan
- ⁶⁶ IJCLab, Université Paris-Saclay, CNRS/IN2P3, 91405 Orsay, France
- ⁶⁷ Centro Nacional de Microelectrónica (IMB-CNM-CSIC), Barcelona, Spain
- ⁶⁸ Department of Physics, Indiana University, Bloomington, IN, USA
- ⁶⁹ ^(a)INFN Gruppo Collegato di Udine, Sezione di Trieste, Udine, Italy; ^(b)ICTP, Trieste, Italy; ^(c)Dipartimento Politecnico di Ingegneria e Architettura, Università di Udine, Udine, Italy
- ⁷⁰ ^(a)INFN Sezione di Lecce, Lecce, Italy; ^(b)Dipartimento di Matematica e Fisica, Università del Salento, Lecce, Italy
- ⁷¹ ^(a)INFN Sezione di Milano, Milan, Italy; ^(b)Dipartimento di Fisica, Università di Milano, Milan, Italy
- ⁷² ^(a)INFN Sezione di Napoli, Naples, Italy; ^(b)Dipartimento di Fisica, Università di Napoli, Naples, Italy

- 73 (a) INFN Sezione di Pavia, Pavia, Italy; (b) Dipartimento di Fisica, Università di Pavia, Pavia, Italy
- 74 (a) INFN Sezione di Pisa, Pisa, Italy; (b) Dipartimento di Fisica E. Fermi, Università di Pisa, Pisa, Italy
- 75 (a) INFN Sezione di Roma, Rome, Italy; (b) Dipartimento di Fisica, Sapienza Università di Roma, Rome, Italy
- 76 (a) INFN Sezione di Roma Tor Vergata, Rome, Italy; (b) Dipartimento di Fisica, Università di Roma Tor Vergata, Rome, Italy
- 77 (a) INFN Sezione di Roma Tre, Rome, Italy; (b) Dipartimento di Matematica e Fisica, Università Roma Tre, Rome, Italy
- 78 (a) INFN-TIFPA, Povo, Italy; (b) Università degli Studi di Trento, Trento, Italy
- 79 Department of Astro and Particle Physics, Universität Innsbruck, Innsbruck, Austria
- 80 University of Iowa, Iowa City, IA, USA
- 81 Department of Physics and Astronomy, Iowa State University, Ames, IA, USA
- 82 Istinye University, Sariyer, Istanbul, Türkiye
- 83 (a) Departamento de Engenharia Elétrica, Universidade Federal de Juiz de Fora (UFJF), Juiz de Fora, Brazil; (b) Universidade Federal do Rio de Janeiro COPPE/EE/IF, Rio de Janeiro, Brazil; (c) Instituto de Física, Universidade de São Paulo, São Paulo, Brazil; (d) Rio de Janeiro State University, Rio de Janeiro, Brazil
- 84 KEK, High Energy Accelerator Research Organization, Tsukuba, Japan
- 85 Graduate School of Science, Kobe University, Kobe, Japan
- 86 (a) AGH University of Krakow, Faculty of Physics and Applied Computer Science, Krakow, Poland; (b) Marian Smoluchowski Institute of Physics, Jagiellonian University, Krakow, Poland
- 87 Institute of Nuclear Physics Polish Academy of Sciences, Krakow, Poland
- 88 Faculty of Science, Kyoto University, Kyoto, Japan
- 89 Research Center for Advanced Particle Physics and Department of Physics, Kyushu University, Fukuoka, Japan
- 90 Instituto de Física La Plata, Universidad Nacional de La Plata and CONICET, La Plata, Argentina
- 91 Physics Department, Lancaster University, Lancaster, UK
- 92 Oliver Lodge Laboratory, University of Liverpool, Liverpool, UK
- 93 Department of Experimental Particle Physics, Jožef Stefan Institute and Department of Physics, University of Ljubljana, Ljubljana, Slovenia
- 94 School of Physics and Astronomy, Queen Mary University of London, London, UK
- 95 Department of Physics, Royal Holloway University of London, Egham, UK
- 96 Department of Physics and Astronomy, University College London, London, UK
- 97 Louisiana Tech University, Ruston, LA, USA
- 98 Fysiska institutionen, Lunds universitet, Lund, Sweden
- 99 Departamento de Física Teórica C-15 and CIAFF, Universidad Autónoma de Madrid, Madrid, Spain
- 100 Institut für Physik, Universität Mainz, Mainz, Germany
- 101 School of Physics and Astronomy, University of Manchester, Manchester, UK
- 102 CPPM, Aix-Marseille Université, CNRS/IN2P3, Marseille, France
- 103 Department of Physics, University of Massachusetts, Amherst, MA, USA
- 104 Department of Physics, McGill University, Montreal, QC, Canada
- 105 School of Physics, University of Melbourne, Victoria, Australia
- 106 Department of Physics, University of Michigan, Ann Arbor, MI, USA
- 107 Department of Physics and Astronomy, Michigan State University, East Lansing, MI, USA
- 108 Group of Particle Physics, University of Montreal, Montreal, QC, Canada
- 109 Fakultät für Physik, Ludwig-Maximilians-Universität München, Munich, Germany
- 110 Max-Planck-Institut für Physik (Werner-Heisenberg-Institut), Munich, Germany
- 111 Graduate School of Science and Kobayashi-Maskawa Institute, Nagoya University, Nagoya, Japan
- 112 Department of Physics and Astronomy, University of New Mexico, Albuquerque, NM, USA
- 113 Institute for Mathematics, Astrophysics and Particle Physics, Radboud University/Nikhef, Nijmegen, The Netherlands
- 114 Nikhef National Institute for Subatomic Physics and University of Amsterdam, Amsterdam, The Netherlands
- 115 Department of Physics, Northern Illinois University, DeKalb, IL, USA
- 116 (a) New York University Abu Dhabi, Abu Dhabi, United Arab Emirates; (b) University of Sharjah, Sharjah, United Arab Emirates
- 117 Department of Physics, New York University, New York, NY, USA
- 118 Ochanomizu University, Otsuka, Bunkyo-ku, Tokyo, Japan
- 119 Ohio State University, Columbus, OH, USA

- 120 Homer L. Dodge Department of Physics and Astronomy, University of Oklahoma, Norman, OK, USA
- 121 Department of Physics, Oklahoma State University, Stillwater, OK, USA
- 122 Joint Laboratory of Optics, Palacký University, Olomouc, Czech Republic
- 123 Institute for Fundamental Science, University of Oregon, Eugene, OR, USA
- 124 Graduate School of Science, Osaka University, Osaka, Japan
- 125 Department of Physics, University of Oslo, Oslo, Norway
- 126 Department of Physics, Oxford University, Oxford, UK
- 127 LPNHE, Sorbonne Université, Université Paris Cité, CNRS/IN2P3, Paris, France
- 128 Department of Physics, University of Pennsylvania, Philadelphia, PA, USA
- 129 Department of Physics and Astronomy, University of Pittsburgh, Pittsburgh, PA, USA
- 130 ^(a)Laboratório de Instrumentação e Física Experimental de Partículas-LIP, Lisbon, Portugal; ^(b)Departamento de Física, Faculdade de Ciências, Universidade de Lisboa, Lisbon, Portugal; ^(c)Departamento de Física, Universidade de Coimbra, Coimbra, Portugal; ^(d)Centro de Física Nuclear da Universidade de Lisboa, Lisbon, Portugal; ^(e)Departamento de Física, Universidade do Minho, Braga, Portugal; ^(f)Departamento de Física Teórica y del Cosmos, Universidad de Granada, Granada, Spain; ^(g)Departamento de Física, Instituto Superior Técnico, Universidade de Lisboa, Lisbon, Portugal
- 131 Institute of Physics of the Czech Academy of Sciences, Prague, Czech Republic
- 132 Czech Technical University in Prague, Prague, Czech Republic
- 133 Charles University, Faculty of Mathematics and Physics, Prague, Czech Republic
- 134 Particle Physics Department, Rutherford Appleton Laboratory, Didcot, UK
- 135 IRFU, CEA, Université Paris-Saclay, Gif-sur-Yvette, France
- 136 Santa Cruz Institute for Particle Physics, University of California Santa Cruz, Santa Cruz, CA, USA
- 137 ^(a)Departamento de Física, Pontificia Universidad Católica de Chile, Santiago, Chile; ^(b)Millennium Institute for Subatomic Physics at High Energy Frontier (SAPHIR), Santiago, Chile; ^(c)Instituto de Investigación Multidisciplinario en Ciencia y Tecnología y Departamento de Física, Universidad de La Serena, La Serena, Chile; ^(d)Department of Physics, Universidad Andres Bello, Santiago, Chile; ^(e)Instituto de Alta Investigación, Universidad de Tarapacá, Arica, Chile; ^(f)Departamento de Física, Universidad Técnica Federico Santa María, Valparaíso, Chile
- 138 Department of Physics, University of Washington, Seattle, WA, USA
- 139 Department of Physics and Astronomy, University of Sheffield, Sheffield, UK
- 140 Department of Physics, Shinshu University, Nagano, Japan
- 141 Department Physik, Universität Siegen, Siegen, Germany
- 142 Department of Physics, Simon Fraser University, Burnaby, BC, Canada
- 143 SLAC National Accelerator Laboratory, Stanford, CA, USA
- 144 Department of Physics, Royal Institute of Technology, Stockholm, Sweden
- 145 Departments of Physics and Astronomy, Stony Brook University, Stony Brook, NY, USA
- 146 Department of Physics and Astronomy, University of Sussex, Brighton, UK
- 147 School of Physics, University of Sydney, Sydney, Australia
- 148 Institute of Physics, Academia Sinica, Taipei, Taiwan
- 149 ^(a)E. Andronikashvili Institute of Physics, Iv. Javakhishvili Tbilisi State University, Tbilisi, Georgia; ^(b)High Energy Physics Institute, Tbilisi State University, Tbilisi, Georgia; ^(c)University of Georgia, Tbilisi, Georgia
- 150 Department of Physics, Technion, Israel Institute of Technology, Haifa, Israel
- 151 Raymond and Beverly Sackler School of Physics and Astronomy, Tel Aviv University, Tel Aviv, Israel
- 152 Department of Physics, Aristotle University of Thessaloniki, Thessaloniki, Greece
- 153 International Center for Elementary Particle Physics and Department of Physics, University of Tokyo, Tokyo, Japan
- 154 Department of Physics, Tokyo Institute of Technology, Tokyo, Japan
- 155 Department of Physics, University of Toronto, Toronto, ON, Canada
- 156 ^(a)TRIUMF, Vancouver, BC, Canada; ^(b)Department of Physics and Astronomy, York University, Toronto, ON, Canada
- 157 Division of Physics and Tomonaga Center for the History of the Universe, Faculty of Pure and Applied Sciences, University of Tsukuba, Tsukuba, Japan
- 158 Department of Physics and Astronomy, Tufts University, Medford, MA, USA
- 159 United Arab Emirates University, Al Ain, United Arab Emirates
- 160 Department of Physics and Astronomy, University of California Irvine, Irvine, CA, USA
- 161 Department of Physics and Astronomy, University of Uppsala, Uppsala, Sweden
- 162 Department of Physics, University of Illinois, Urbana, IL, USA

- ¹⁶³ Instituto de Física Corpuscular (IFIC), Centro Mixto Universidad de Valencia-CSIC, Valencia, Spain
- ¹⁶⁴ Department of Physics, University of British Columbia, Vancouver, BC, Canada
- ¹⁶⁵ Department of Physics and Astronomy, University of Victoria, Victoria, BC, Canada
- ¹⁶⁶ Fakultät für Physik und Astronomie, Julius-Maximilians-Universität Würzburg, Würzburg, Germany
- ¹⁶⁷ Department of Physics, University of Warwick, Coventry, UK
- ¹⁶⁸ Waseda University, Tokyo, Japan
- ¹⁶⁹ Department of Particle Physics and Astrophysics, Weizmann Institute of Science, Rehovot, Israel
- ¹⁷⁰ Department of Physics, University of Wisconsin, Madison, WI, USA
- ¹⁷¹ Fakultät für Mathematik und Naturwissenschaften, Fachgruppe Physik, Bergische Universität Wuppertal, Wuppertal, Germany
- ¹⁷² Department of Physics, Yale University, New Haven, CT, USA
- ^a Also at Affiliated with an Institute Covered by a Cooperation Agreement with CERN, Geneva, Switzerland
- ^b Also at An-Najah National University, Nablus, Palestine
- ^c Also at Borough of Manhattan Community College, City University of New York, New York, NY, USA
- ^d Also at Center for High Energy Physics, Peking University, Beijing, China
- ^e Also at Center for Interdisciplinary Research and Innovation (CIRI-AUTH), Thessaloniki, Greece
- ^f Also at Centro Studi e Ricerche Enrico Fermi, Rome, Italy
- ^g Also at CERN, Geneva, Switzerland
- ^h Also at Département de Physique Nucléaire et Corpusculaire, Université de Genève, Geneva, Switzerland
- ⁱ Also at Departament de Física de la Universitat Autònoma de Barcelona, Barcelona, Spain
- ^j Also at Department of Financial and Management Engineering, University of the Aegean, Chios, Greece
- ^k Also at Department of Physics, Ben Gurion University of the Negev, Beer Sheva, Israel
- ^l Also at Department of Physics, California State University, Sacramento, USA
- ^m Also at Department of Physics, King's College London, London, UK
- ⁿ Also at Department of Physics, Stanford University, Stanford CA, USA
- ^o Also at Department of Physics, University of Fribourg, Fribourg, Switzerland
- ^p Also at Department of Physics, University of Thessaly, Thessaly, Greece
- ^q Also at Department of Physics, Westmont College, Santa Barbara, USA
- ^r Also at Hellenic Open University, Patras, Greece
- ^s Also at Institutio Catalana de Recerca i Estudis Avancats, ICREA, Barcelona, Spain
- ^t Also at Institut für Experimentalphysik, Universität Hamburg, Hamburg, Germany
- ^u Also at Institute for Nuclear Research and Nuclear Energy (INRNE) of the Bulgarian Academy of Sciences, Sofia, Bulgaria
- ^v Also at Institute of Applied Physics, Mohammed VI Polytechnic University, Ben Guerir, Morocco
- ^w Also at Institute of Particle Physics (IPP), Toronto, Canada
- ^x Also at Institute of Physics and Technology, Mongolian Academy of Sciences, Ulaanbaatar, Mongolia
- ^y Also at Institute of Physics, Azerbaijan Academy of Sciences, Baku, Azerbaijan
- ^z Also at Institute of Theoretical Physics, Ilia State University, Tbilisi, Georgia
- ^{aa} Also at L2IT, Université de Toulouse, CNRS/IN2P3, UPS, Toulouse, France
- ^{ab} Also at Lawrence Livermore National Laboratory, Livermore, USA
- ^{ac} Also at National Institute of Physics, University of the Philippines Diliman, Diliman, Philippines
- ^{ad} Also at Technical University of Munich, Munich, Germany
- ^{ae} Also at The Collaborative Innovation Center of Quantum Matter (CICQM), Beijing, China
- ^{af} Also at TRIUMF, Vancouver, BC, Canada
- ^{ag} Also at Università di Napoli Parthenope, Naples, Italy
- ^{ah} Also at University of Chinese Academy of Sciences (UCAS), Beijing, China
- ^{ai} Also at Department of Physics, University of Colorado Boulder, Colorado, USA
- ^{aj} Also at Washington College, Chestertown, MD, USA
- ^{ak} Also at Physics Department, Yeditepe University, Istanbul, Türkiye
- * Deceased